

Learning-based 3D Reconstruction in Autonomous Driving: A Comprehensive Survey

Liewen Liao, Weihao Yan, Ming Yang *Member, IEEE*, Songan Zhang*

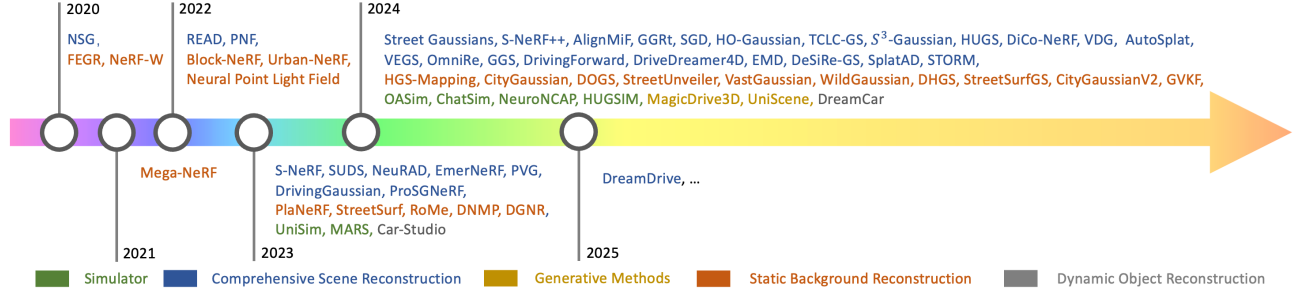


Fig. 1: Learning-based 3D reconstruction researches has witnessed a explosive growth in autonomous driving recent years.

Abstract—Learning-based 3D reconstruction has emerged as a transformative technique in autonomous driving, enabling precise modeling of both dynamic and static environments through advanced neural representations. Despite augmenting perception, 3D reconstruction inspires pioneering solution for vital tasks in the field of autonomous driving, such as scene understanding and closed-loop simulation. Commencing with an examination of input modalities, we investigate the details of 3D reconstruction and conducts a multi-perspective, in-depth analysis of recent advancements. Specifically, we first provide a systematic introduction of preliminaries, including data formats, benchmarks and technical preliminaries of learning-based 3D reconstruction, facilitating instant identification of suitable methods based on hardware configurations and sensor suites. Then, we systematically review learning-based 3D reconstruction methods in autonomous driving, categorizing approaches by subtasks and conducting multi-dimensional analysis and summary to establish a comprehensive technical reference. The development trends and existing challenges is summarized in the context of learning-based 3D reconstruction in autonomous driving. We hope that our review will inspire future researches.

Index Terms—3D Reconstruction, Autonomous Driving, Scene Understanding, Close-loop Simulator

I. INTRODUCTION

AUTONOMOUS driving has garnered significant research attention in recent years due to the advantages in transportation safety and efficiency. This transformative technology fundamentally relies on precise environmental perception and holistic scene understanding, which necessitate large-scale multimodal datasets with sufficient diversity. However, the acquisition of such datasets incurs exorbitant costs while introducing safety risks during data collection, particularly for edge cases. Emerging 3D reconstruction technologies offer a groundbreaking solution to this challenge. By creating photorealistic and geometrically manipulable digital twins of the physical world, 3D reconstruction enables cost-effective acquisition of abundant data. The advent of NeRF in 2020 marked a paradigm shift towards learning-based reconstruction methods,

which demonstrate superior scalability and fidelity compared to hand-crafted modeling or traditional reconstruction approaches. In the context of autonomous driving, learning-based 3D reconstruction has evolved into a foundational technology with applications spanning multiple tasks. Current research advancements extend beyond data augmentation to encompass multimodal sensor simulation, enhanced scene understanding, and closed-loop simulator, demonstrating deep integration across the full autonomy stack.

Parallel to 3D reconstruction methodologies, the emerging paradigm of 2D generative models [68]–[75] demonstrates direct synthesis capabilities for visual media. Comparatively, 3D reconstruction [67], [76]–[82], [98], [111], [113], [115] exhibits critical advantages: **1) Fidelity.** By integrating spatial geometry reconstruction and physically grounded rendering, 3D reconstruction demonstrates superior perceptual fidelity in temporal coherence and cross-modal spatial alignment capabilities. While contemporary 3D reconstruction frameworks increasingly provide multi-modal sensor synchronization, 2D generative methods remain largely limited on single-modal media. **2) Framerate.** The separated optimization-rendering architecture in 3D reconstruction enables real-time rendering [2], [24], [53], [104], [107], contrasting sharply with 2D generative models’ computational bottlenecks that limit rendering to single-digit fps [68], [71]. **3) Flexibility.** 3D reconstruction enables direct parametric control over reconstruction targets, imaging parameters, and spatial layouts with inherent operational flexibility [32], [98], [115], whereas generative methods are confined to conditional synthesis paradigms that demonstrate comparatively constrained controllability [69], [79], [81]. However, driven by the inherent advantages of 2D generative methods in computational efficiency and expressive capacity, recent advancements are exploring synergistic integration of 2D and 3D paradigms to harness their complementary strengths.

Learning-based 3D reconstruction methods in autonomous driving have undergone a transformative technical evolution in

three dimensions: *Data Accessibility*. The field has witnessed a paradigm shift in data requirements, transitioning from demanding calibrated multi-sensor setups [17], [27], [52], [67], [82], [88], [108], [113], [115] (aligned point cloud and image with precise calibration) to enabling 3D reconstruction from uncalibrated image sequences [18], [41], [105], [114]. This relaxation of multimodal constraints significantly enhances data accessibility by supporting crowd-sourced image collection. *Scene Representation Advancements*. 3D scene representation has evolved from explicit geometric primitives [52], [109], [110] and NeRF [65], [66], [98], [112], to 3D Gaussian Splatting [32], [114], [115] and time-varying 4D Gaussians [101], [117], [118], and ultimately to hybrid representations [30], [100] that balance reconstruction quality and speed, reflecting progressive improvement in balancing the quality-efficiency trade-off across successive scene representations. *Methodological Paradigms*. 3D reconstruction paradigm has transitioned from scene-specific optimization in origin NeRF/3D Gaussian Splatting [35], [67], [98], [104], [111] to generalizable modeling with feedforward networks [114], ultimately to generative synthesis with primary guidance [20], [54] (e.g. BEV layouts, text prompts), overcoming scalability limitations through cross-scene priors while enabling photorealistic and semantic-consistent scene creation.

This survey provides a systematic review of learning-based 3D reconstruction technologies tailored to autonomous driving, coupled with a panoramic overview of their applications, to equip practitioners with a holistic understanding of the field. The contribution of this survey can be summarized as follows:

- Introduction of learning-based 3D reconstruction preliminaries encompassing data modalities, benchmarks, and technical preliminaries, enabling rapid algorithmic selection aligned with task-specific requirements
- Systematic summary of related works across different reconstruction scope in driving scene, enabling target-specific multi-perspective analysis and cross-methodological comparison
- Analysis of applications of 3D reconstruction across practical autonomous driving tasks, with emergent technical trends highlighted for future development

The organization of this survey is as follows: First, we introduce data formats and benchmarks for 3D reconstruction in Section II. Second, we present the technical preliminaries of 3D reconstruction including representation and rendering methods in Section III. Third, we introduce milestones of learning-based 3D reconstruction in Section III-C. Subsequently, we systematically examine reconstructions across different scope in driving scene and discuss downstream applications in Section IV. Finally, we trace the evolutionary trajectory of learning-based 3D reconstruction in autonomous driving and critically analyze its persisting technical challenges in Section V.

II. DATA MODALITY & BENCHMARK

A. Data Modality

In autonomous driving, the selection of an optimal 3D reconstruction method is deeply influenced by the input data

modality. Diverse data modalities—including images, depth maps, and point clouds—provide multidimensional scene representations with varying accuracy and computational demands, which in turn affect the performance and choice of reconstruction techniques. This chapter lays the groundwork by thoroughly reviewing the data modality and benchmarks.

Image Image, as the most popular format in vision-based techniques, provides fine-grained details and textures in high resolution. Images typically encapsulate camera parameters—intrinsic (focal length, principal point) and extrinsic (position, orientation)—within their metadata, dubbed calibrated image. Calibration establishes precise imaging models essential for recovering geometry from 2D visual data. For the sake of simplicity, we do not distinguish image and video in this survey, since both of them are encoded in 2D pixel space.

Depth Image Depth maps typically serve as a complement to 2D image, providing a pixel-aligned grayscale representation that encodes the Euclidean distance from each imaged point to the camera’s imaging plane. Their accuracy depends on acquisition methods: Time-of-Flight (ToF) sensors yield high-precision depth maps, whereas stereo or monocular estimation algorithms produce lower-accuracy results with significantly reduced acquisition complexity.

Point Cloud Point cloud is an unordered set of points in space, where each element describes the spatial coordinates of a point on object surface. Unlike depth maps, which represent spatial information through a lossy compressed 2D projection, point clouds preserve the 3D geometric details of an object. Due to their non-structural nature, multiple point clouds can be easily merged into a combined point cloud. However, the absence of explicit topological relations necessitates computationally intensive processing pipelines. Acquisition precision varies significantly across modalities: LiDAR generates high-accuracy point clouds at expensive hardware requirements, Radar provides lower-resolution alternatives, while traditional geometric algorithms (e.g., Structure-from-Motion, Multi-View Stereo) offer compromised solutions for depth estimation from multi-view images when direct 3D sensing is unavailable.

B. Datasets

Datasets serve as the cornerstone for training and evaluating learning-based 3D reconstruction algorithms. This chapter categorizes key datasets into three groups: static background datasets emphasizing infrastructure reconstruction, vehicle datasets, and comprehensive datasets for composite scene reconstruction with both static background and dynamic agents, highlighting their distinct roles in advancing scene completeness, geometric fidelity, and temporal coherence in autonomous driving applications. For an exhaustive autonomous driving dataset survey, we refer readers to [136].

1) *Comprehensive Datasets*: 3D reconstruction of autonomous driving scenes demands datasets that holistically encapsulate both static environments and dynamic agents, mirroring real-world complexity. Comprehensive datasets typically encompass temporally continuous image sequences or video streams, often augmented with LiDAR point clouds,

Dataset	Year	Type	Modality			Annotation		Volume		Resolution	Frame Rate		Sem. Types	Weather Types	Time of Day	Scenario Types
			Image	Depth	PCL	BBox	Semantic	Scenes	Image		Camera	LiDAR				
KITTI [83]	2012	Real	✓	✓	✓	3D	0	22	15K	1242×376	10	10	8	1	1	2
SemanticKITTI [84]	2019	Real	-	-	✓	-	✓	22	43552	-	-	10	28	1	1	4
VirtualKITTI2 [85]	2020	Syn.	✓	✓	-	3D	✓	5	20992	1242×375	#	-	8	3	2	5
KITTI-360 [86]	2022	Real	✓	-	✓	3D	✓	11	150K	1408×376	#	#	37	1	1	1
NuScenes [141]	2019	Real	✓	-	✓	3D	✓	1000	1.4M	2048×1536	12	10	23	3	2	4
Waymo [142]	2019	Real	✓	-	✓	3D	✓	1150	390K	1920×1080	10	10	23	2	3	5
NOTR [82]	2023	Real	✓	-	✓	3D	✓	120	#	1920×1080	10	10	23	#	#	#
BDD100K [140]	2018	Real	✓	-	-	2D	✓	100k	12M	1280×720	30	-	40	5	2	4
Argoverse2 [151]	2021	Real	✓	-	✓	3D	✓	1000	6M	2048×1550	20	10	30	2	1	1
XLD [37]	2024	Syn.	✓	-	✓	-	✓	6	3600	1920×1080	#	#	#	#	#	6

TABLE I: Overall comparison between comprehensive datasets. “-” indicates the absence of this modality, “#” indicates not officially mentioned. “3D” denotes bounding box annotations with spatial coordinates, “2D” indicates annotations only in the image space.

alongside rich metadata such as sensor calibration parameters, 2D/3D bounding box annotations, and HD maps, enabling joint modeling of infrastructure permanence and object motion. These datasets challenge algorithms to resolve cross-modal ambiguities while preserving geometric-temporal coherence, serving as universal evaluation of 3D reconstruction approaches.

KITTI [83], released in 2013, is one of the most influential datasets in the field of autonomous driving. However, KITTI’s limited diversity in weather conditions, day of time, scenario types, and merely eight semantic categories fails to adequately represent real-world driving complexity.

VirtualKITTI 2 [85] is a synthetic datasets generated from 5 virtual worlds in urban settings, two of which are recreations from the KITTI dataset. VirtualKITTI 2 includes a variety of weather conditions and times of day, enhancing data diversity compared to KITTI.

SemanticKITTI [84], as an extension of KITTI released in 2019, focuses on semantic segmentation of LiDAR point clouds. The dataset provides enlarged semantic categories, ranging from ground, building, vehicle, and human. It is designed to support research in 3D semantic segmentation and scene understanding.

KITTI-360 [86], proposed in 2020, upgrades the KITTI framework with enhanced quality and FoV. Key advancements include strict sensor synchronization, expanded vertical FoV, panoramic coverage eliminating blind spots, and open-source calibration tools.

NuScenes [141] constitutes a milestone in autonomous driving research, delivering a synchronized 360° multimodal data with full sensor suite, semantic and 3D bounding box annotation in both image and point cloud, and accurate human-annotated HD map, facilitating wide-range downstream tasks, especially for panoramic-based techniques. However, NuScenes remains technically constrained by inadequate LiDAR resolution and restricted vertical FoV.

Waymo Open Perception Dataset [142] represents another seminal multimodal benchmark in autonomous driving research, distinguished by its expanded LiDAR coverage with superior point cloud resolution, diversified 2D/3D annotation taxonomies, and extensive geographical diversity. However, the absence of backward-facing camera modules breaks the perceptual integrity that constrain its applicability in holistic environmental perception tasks.

NOTR [82] curates a subset of Waymo Open Dataset characterized by heterogeneous traffic states, weather conditions, and temporal variations. Enhanced with supplementary annotations, NOTR strengthens enables rigorous evaluation of reconstruction robustness and generalization across downstream tasks.

BDD100K [140] developed by UC Berkeley in 2018, focuses on vision-centric driving comprehension. BDD100K surpasses existing datasets in data scale, providing a significantly larger volume of annotated driving scene data, but only contains 2D data and limited metadata, lacking 3D information and precise camera poses, which makes it challenging for training. Nonetheless, its diversity makes it an excellent dataset for testing model generalization.

Argoverse2 [151] emerges as the largest multimodal autonomous driving dataset to date, encompassing heterogeneous weather conditions, varying illumination and geographic diversity across six cities. While providing synchronized multi-sensor streams and auxiliary annotations including HD vector maps and 3D object detections, the dataset deliberately omits 2D/3D semantic segmentation labels, thereby prioritizing self-supervised learning paradigms over supervised approaches.

XLD [37] constitutes a dedicated benchmark for novel view synthesis in autonomous driving, specifically engineered to capture lateral lane-changing maneuvers. It provides fine-grained testing perspectives encompassing 1, 2, 4 meter lateral offsets from initial positions, coupled with diverse weather conditions and times of day. The dataset addresses the critical gap of missing ground-truth novel views in existing benchmarks, enables quantitative evaluation for downstream tasks including closed-loop simulation and perception system validation.

2) *Static Scene Dataset*: Considering the inherent structural homogeneity of urban environments and static background of driving scenarios, we further contextualize datasets tailored for urban scene 3D reconstruction. These datasets typically comprise large-scale urban infrastructure image (e.g., buildings, road networks) and LiDAR scans, demanding methodologies that prioritize accurate recovery of static background elements while addressing challenges like multi-scale geometric patterns and occlusion resilience.

Quad6K [139], constructed from imagery of Cornell University’s Arts Quad, comprises geotagged images alongside SfM reconstructions. While pioneering in early 3D recon-

struction research, Quad6K’s limited annotation granularity and dated sensor specifications render its utility obsolete for modern benchmarks requiring detailed geometry validation or cross-modal alignment in complex urban scenarios.

UrbanScene3D [134] offers both real and synthetic large-scale urban scenes with synchronized LiDAR and camera across diverse conditions. Featuring fine-grained supplementary annotations, it enables robust 3D perception benchmarking—supporting reconstruction, motion prediction, and scene completion tasks through geometrically precise multi-sensor recordings. However, the large-scale urban environments in these datasets are synthesized with CAD, resulting in diminished authenticity and loss of fine-grained geometric details.

MatrixCity [135], a large-scale synthetic urban dataset built on Unreal Engine, provides RGB-D imagery and corresponding point clouds with controlled diverse environmental conditions (weather, lighting) and material information. It uniquely integrates aerial and street-view perspectives to broaden task applicability. However, the lack of supplementary annotation metadata (semantic/instance labels) constrains its utility for downstream tasks requiring supervised learning.

Mill-19 [4] is proposed in Mega-NeRF, providing high-resolution images for two mid-size real industrial scenes captured by drone. While Mill-19 partially addresses data gaps in suburban and industrial areas environments, it exhibits notable limitations including sparse scene diversity and the absence of LiDAR data.

3) *Vehicle Dataset*: Vehicle datasets exhibit limited availability, primarily stemming from the inherent diversity of vehicle categories, annual model variants, and significant appearance variations within same models, which collectively pose substantial challenges for complete data acquisition and precise annotation.

CarPatch3D [137] collects 530,101 car patches from 206,403 instances of three public datasets along with the corresponding binary mask generated by SAM [91], estimated camera parameters, 3D position and orientation of the vehicles predicted by DD3D [138]. CarPatch3D establishes the first specialized dataset for vehicle, yet exhibits inherent quality variance due to its image-cropped acquisition methodology.

3DRealCar [46] is a large-scale 3D vehicle dataset containing 2,500 cars. It provides high-quality data captured by 3D scanners, including RGB-D images and point clouds under three different lighting conditions: reflective, standard, and dark. Additionally, it offers fine-grained two-dimensional semantic segmentation annotations, providing solid foundation of vehicle 3D reconstruction.

Dataset	Year	Type	View	Image	PCL	Annotation		Vol.	Res.
						BBox	Semantic		
Quad6K	2016	Real	A	✓	-	-	-	6514	1708×1329
UrbanScene3D	2022	Real+Syn.	A	✓	✓	2D/3D	✓	128k	5472×3648
MatrixCity	2023	Syn.	A+S	✓	✓	-	-	519K	1920×1080
Mill-19	2022	Real	A	✓	-	-	-	3.6K	4608×3456

TABLE II: Comparison between static datasets. "A" indicates aerial view, "S" indicates street view.

C. Metrics

MSE Mean square error (MSE) is the most popular metric to measure the average square difference between the predicted value \hat{y}_i and the ground truth value y_i , which is defined as:

$$MSE = \frac{1}{n} \sum_{i=1}^n (y_i - \hat{y}_i)^2 \quad (1)$$

MSE calculates the pixel-level difference without normalization, which makes it less intuitive for reflecting human perception of image quality. Thus, MSE is more suitable as a loss function rather than an evaluation metric for 3D reconstruction.

PSNR Peak Signal-to-Noise Ratio (PSNR) is used to measure the quality of reconstructed images by comparing them to the original reference. PSNR is derived from MSE by calculating the ratio between the maximum possible pixel value and the MSE between two images. PSNR in dB is defined as:

$$PSNR = 10 \cdot \log_{10} \left(\frac{MAX^2}{MSE} \right) \quad (2)$$

where MAX is the maximum pixel value (e.g. 255 for 8-bit image). PSNR is widely used due to its simplicity and ease of calculation, but it retains the pixel-level computation characteristic from MSE, which leads to incapable of capturing structural distortions.

SSIM Structural Similarity Index (SSIM) evaluates the similarity between two images based on three aspects: luminance, contrast and structure, which is defined as:

$$l(x, y) = \frac{2\mu_x\mu_y}{\mu_x^2 + \mu_y^2}, c(x, y) = \frac{2\sigma_x\sigma_y}{\sigma_x^2 + \sigma_y^2}, s(x, y) = \frac{\sigma_{xy}}{\sigma_x\sigma_y}$$

$$SSIM(x, y) = l(x, y) \cdot c(x, y) \cdot s(x, y) = \frac{(2\mu_x\mu_y)(2\sigma_{xy})}{(\mu_x^2 + \mu_y^2)(\sigma_x^2 + \sigma_y^2)}$$

where x and y are two images being compared, μ_x and μ_y are the means, σ_x^2 and σ_y^2 are the variance of x and y respectively, σ_{xy} is the covariance of x and y . SSIM can better reflect human perceptual quality and capture local structural information, but it also brings a greater computational load and still cannot reflect global structural information.

LPIS Learned Perceptual Image Patch Similarity [153] uses pretrained deep convolutional models (e.g. VGG [8] or AlexNet [9]) to extract multi-scale features from image and computes the similarity between features. Since LPIS involves comparisons of deep features in its calculations, it can better reflect global structural and high-level semantic information and align more closely with human perceptual results. However, the computation of LPIS relies on pre-trained deep models, which makes its more computational intensive than SSIM. Moreover, LPIS may not capture all types of distortions, especially features not well-learned in pretrained models.

IS Inception Score [154] evaluates the quality of generated images in downstream tasks (e.g. novel view synthesis) by measuring the diversity and clarity of classification from a pre-trained Inception model:

$$IS(G) = \exp(\mathbb{E}_{x \sim p_g} D_{KL}(p(y|x) \| p(y))) \quad (3)$$

Higher IS indicates the input image distribution is more close to the distribution used for pre-training, i.e. nature images.

FID Fréchet Inception Distance [155] is a metric used to evaluate the quality of generated image. It quantifies the similarity between the distributions of generated image and real image with a pre-trained Inception V3 [7] model. Features extracted by the pre-trained model is assumed to follow a multivariate Gaussian distribution. Thus, FID is calculated with the mean and covariance of the two distributions:

$$FID = \|\mu_r - \mu_g\|^2 + \text{Tr}(\Sigma_r + \Sigma_g - 2(\Sigma_r \Sigma_g)^{1/2}) \quad (4)$$

where μ_r and μ_g are the mean vectors, Σ_r and Σ_g are the covariance matrices of the real and generated image distributions respectively. FID provides a more comprehensive evaluation by considering the distribution of high-level features, making it sensitive to both the quality and diversity of the generated images. But FID is limited by its high computational complexity arise from feature extraction with Inception V3.

III. PRELIMINARY

A. Representation

Representation serves as the informational substrate that fundamentally determines both the reconstruction fidelity and computational efficiency. Representation can be categorized into two main types: implicit and explicit representations. By examining each representation in detail, we aim to shed light on their respective pros and cons.

1) Implicit Representation:

Implicit Surfaces Implicit surfaces leverage equations to describe the surface of objects, such as Bézier surfaces [156]–[158], Non-Uniform Rational B-Splines(NURBS) [159], [160]. Implicit surfaces provide infinite resolution at arbitrary position, making them highly suitable for scenarios that require extremely high precision. However, implicit surfaces suffer from the prohibitive complexity [157] as the geometry details grow which hinders the application in practical scenarios.

Signed Distance Field Signed Distance Field (SDF) describes a function that maps a target location (x, y, z) to the the minimum distance from the location to the surface of object d : $\mathcal{F}(x, y, z) \rightarrow d$. SDF mathematically defines object geometry with compact and versatile representations, where negative, zero, and positive values correspond to interior regions, surface boundaries, and exterior spaces respectively. SDF provides an efficient option for downstream applications that rely solely on geometric features while disregarding visual patterns such as collision calculation [168]–[170] or shape representation [161], [171], [172].

Neural Radiance Field Neural radiance field (NeRF) [56] maps a combination of a target position (x, y, z) and viewing direction (θ, ϕ) , to the volume density and radiance of the target point. NeRF pioneers volumetric neural representations to synthesize photorealistic novel views by optimizing continuous scene functions in differentiable manner, revolutionizing 3D reconstruction. Despite its advantages, the methodology introduces substantial computational overheads from sampling inefficiency and ambiguous optimization constraints, while incurring significant inference latency that poses critical challenges in real-time rendering pipelines.

2) Explicit Representation:

Point Cloud A 3D point cloud is an unordered collection of data points, typically representing the surface of an object or scene due to the acquisition methods. Each point consists of coordinates $\mathbf{x} \in \mathbb{R}^3$ and additional attributes such as color \mathbf{c} , intensity σ , or normal vectors \vec{n} . Point cloud, typically obtained through 3D sensing modalities like LiDAR/Radar, exhibits operational flexibility for aggregation/fragmentation due to their unstructured nature, while the absence of topological relationships induces elevated computational demands in downstream processing workflows.

Voxel Voxel contains grid-aligned 3D units storing attributes like density or color, enabling structured volumetric discretization with inherent endoluminal characterization, rendering them particularly advantageous for biomedical domains requiring simultaneous surface and internal analysis. Voxels demonstrate application-specific flexibility through different attribute configurations, such as embedding occupancy probability distributions and semantic labels for occupancy grid in autonomous driving, or incorporating learnable features as latent spatial representations in neural network architectures.

Mesh Mesh is a structured representation of 3D surfaces, composed of mesh vertices $\mathcal{V} = \{v_i | i = 1, \dots, N\}$, edges, and faces (typically triangles or polygons). Due to the planar structure of face units, mesh projection and rasterization achieves improved trade-off between fidelity and computational efficiency compared to point cloud, facilitating broad applications in computer graphics and engineering disciplines. However, due to the discrete planar representation of face units, meshes may lose geometric details when modeling complex structures. To reduce accuracy loss, the mesh density often needs to be greatly increased, which inevitably incurs high computational cost.

3D Gaussian Splatting 3D Gaussian Splatting represents the scene with a set of learnable Gaussian distributions with parameterized mean, covariance, opacity and color $\mathcal{G} = \{g(\mu, \Sigma, \sigma, \mathbf{c})\}$. 3DGS advances point cloud representation by equipping each element with enhanced learnable parameters, significantly improving both the information density and expressive capability of individual components. Concurrently, by integrating the computational efficiency and projection accuracy inherent to Gaussian distributions, this approach synergistically achieves dual advantages: higher rendering fidelity and lower computational overhead compared to conventional methods. The combination of these strengths not only enables real-time high-quality visual outputs but also drives diverse downstream applications, positioning 3DGS as the leading 3D representation framework in both research and practical implementations.

B. Differentiable Rendering Methods

Differentiable rendering techniques bridges supervision and learnable parameters of scene representations in a differentiable manner, facilitating modern GPU and gradient-based optimization algorithms in 3D reconstruction. The choice of rendering method deeply influenced the computational efficiency of reconstruction methods.

Rasterization Rasterization converts 3D geometric primitives into discrete pixel fragments for 2D display. The process initiates by transforming 3D spatial coordinates into normalized device coordinates via projection matrices, followed by perspective division to map them to pixel space. Rasterization enables real-time rendering with specific primitives such as triangle or polygon meshes, making it suitable for latency-sensitive tasks. However, rasterization predominantly employs simplified lighting models, which fundamentally restricts its capacity to accurately simulate complex material behaviors. This inherent limitation necessitates computationally intensive approximation algorithms, often resulting in suboptimal rendering fidelity for advanced optical phenomena such as surface reflections and light transmittance through translucent materials.

Volume Rendering Volume rendering is a visualization technique for 3D scalar fields in voxel representation, actively sampling the volume into a 2D image plane through ray-marching or ray-casting. Rays cast from the viewpoint traverse the volume with each ray representing a pixel and sampling points at discrete position within volume, where each point is parameterized by color and opacity. Pixel color is obtained by alpha-blending all sampling points along the ray through opacity-weighted accumulation. Volumetric rendering achieves photorealistic results through physically-grounded simulation of light transport phenomena, while maintaining compatibility with diverse camera models via parameterized projection matrices. However, the dual challenges of suboptimal sampling efficiency and the computational intensity inherent in physically-accurate material simulations—though technically supported—impose significant computational demands that hinder real-time rendering deployment.

C. Learning-based Milestones

NeRF and 3D Gaussian Splatting constitute pivotal milestones in learning-based 3D reconstruction, as NeRF ignited the field’s renaissance while 3DGS further propels it to an unprecedented height across both academic research and practical applications. Subsequently, we provide systematical introduction of these revolutionary frameworks. Figure III-C shows overall framework of these milestones.

Neural Radiance Field (NeRF) represents the scene with a continuous 5D function, mapping the target position (x, y, z) and viewing direction $\mathbf{d} = (\theta, \phi)$ to the opacity σ and color \mathbf{c} of the target: $\mathcal{F}(x, y, z, \theta, \phi) \rightarrow (\sigma, \mathbf{c})$. The original NeRF [56] utilizes a MLP as the implementation of this function. NeRF typically employs ray-marching as the implementation of volume rendering. Given one of the rays emitted from the viewpoint \mathbf{o} with direct \mathbf{d} , termed as $\mathbf{r}(t) = \mathbf{o} + t\mathbf{d}$, the result color \mathbf{C}_r of the corresponding pixel of the ray \mathbf{r} is synthesized through alpha-blending integration of all sampled points in distance order along the ray. Each point contributes radiance based on its opacity σ and color \mathbf{c} :

$$\mathbf{C} = \sum_{i=1}^N (\mathbf{c}_i \cdot \alpha_i \cdot \prod_{j=1}^{i-1} (1 - \alpha_j)) \quad (5)$$

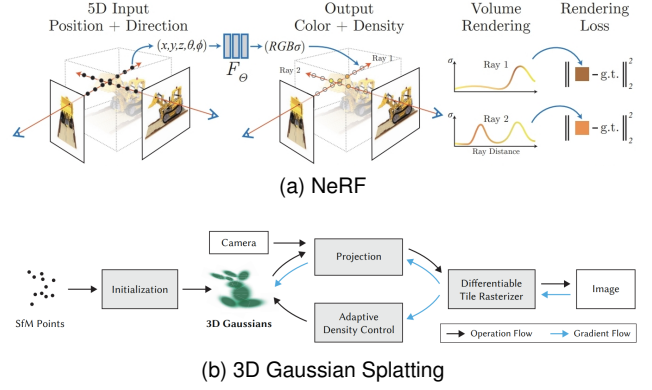


Fig. 2: Framework of NeRF [56] and 3D Gaussian Splatting [64]

Where subscription i denotes the i -th sampling point in near-to-far order.

3D Gaussian Splatting (3DGS) [64] uses a collection of differentiable 3D Gaussian distributions to represent scenes or objects. Each Gaussian $\mathbf{g} = \{\boldsymbol{\mu}, \Sigma, \sigma, \mathbf{c}\}$ is determined by following parameterized attributes: mean position $\boldsymbol{\mu} \in \mathbb{R}^3$, covariance Σ is decomposed into rotation in quaternion $\mathbf{q} \in \mathbb{R}^4$ and anisotropic scale $\mathbf{s} \in \mathbb{R}_+^3$, opacity σ , color \mathbf{c} . Color \mathbf{c} is represented in a view-dependent spherical harmonics (SH). During rendering, these Gaussians are projected onto the 2D image plane as follows:

$$\Sigma' = \mathbf{J}\mathbf{W}\Sigma\mathbf{W}^T\mathbf{J}^T \quad (6)$$

where Σ is the covariance matrix of 3D Gaussian, Σ' is the covariance matrix of the result 2D Gaussian, \mathbf{J} is the Jacobian of the affine approximation of the projective transformation, \mathbf{W} is the viewing transformation. The imaging plane is discretized into pixels akin to rasterization, while within each pixel region, 2D Gaussians undergo alpha-blending analogous to volume rendering in a near-to-far order but Gaussian density serves as opacity:

$$\mathbf{C} = \sum_{i=1}^N (\mathbf{c}_i \cdot \alpha_i \cdot \prod_{j=1}^{i-1} (1 - \alpha_j)), \alpha_i \sim N(\mu_i, \Sigma_i) \quad (7)$$

. This hierarchical compositing synthesizes the final pixel color by accumulating contributions from overlapping splats, weighted by their spatially varying opacity.

IV. RECONSTRUCTION AND APPLICATION

In this section, we present three distinct reconstruction categories differentiated by their scopes: static backgrounds, dynamic objects, and comprehensive scenes combining both elements. We summarize and compare the relevant methods from multiple perspectives according to the characteristics of each category. Static scene reconstruction approaches are summarized in Table III, and an overall comparison among comprehensive scene reconstruction methods, generation methods and simulators is shown in Table IV.

Method	Input			Occl. Idn.	Par. Cri.	Output					Scene Repre.	Dataset					Release	Open Source	
	Image	Pose	PCL			Image	Depth	Normal	Point Cloud	Semantic		Mesh	KITTI	NuScenes	Waymo	KITTI-360			Mill-19
FEGR [5]	✓	✓	A	Sem.	Spa.	✓	✓	✓		✓	NeRF		✓			NeRF-OSR [166], RoadData	20/08		
NeRF-W [102]	✓	✓	-	Uncer.		✓	✓				NeRF						Phototourism [167]	20/08	U
Mega-Nerf [4]	✓	✓	-	Sem.		✓	✓				NeRF			✓	✓		Quad 6k [139]	21/12	✓
Urban-NeRF [55]	✓	✓	S	Sem.		✓	✓			✓	NeRF					The Street View [55], Tanks and Temples [165]	22/06		
Block-NeRF [103]	✓	✓		Sem.	Spa.	✓					NeRF					Customized	22/02	U	
StreetSurf [90]	✓	✓	A		Dist.	✓	✓	✓	✓	✓	NeRF	✓	✓	✓			23/06	✓	
PlaNeRF [25]	✓	✓	-	Sem.		✓	✓		✓	✓	NeRF			✓			23/05		
AlignMiF [26]	✓	✓	I	Sem.		✓	✓		✓		NeRF			✓	✓		24/02	✓	
NeRF On-the-go [49]	✓	✓	-	Uncer.		✓					NeRF			✓		AIODrive [148], NeRF On-the-go [49], RobustNeRF [50]	24/05		
Neural Point Light Field [110]	✓	✓	I			✓	✓		✓		PCL	✓	✓	✓		Cityscapes [143], Argoverse [150]	22/06	✓	
DGMR [31]	✓	✓	-			✓					PCL	✓	✓	✓			23/11		
DNMP [109]	✓	✓	I			✓	✓		✓	✓	Mesh			✓			23/10	✓	
RoMe [51]	✓	✓	-	Sem.	Smpl.	✓	✓		✓	✓	Mesh	✓	✓				23/06	✓	
WildGaussian [92]	✓	✓	I	Uncer.		✓					G. S.					NeRF On-the-go [49], Phototourism [167]	24/07	✓	
VastGaussian [89]	✓	✓	I		Spa.	✓					G. S.				✓		24/06	U	
DHGS [30]	✓	✓	I	Sem.	Dist.	✓	✓		✓		G. S.		✓			NOTR [82]	24/07		
CityGaussian [2]	✓	✓	I		Spa.	✓					G. S.				✓	✓	24/04	✓	
CityGaussianV2 [3]	✓	✓	I		Spa.	✓	✓	✓		✓	G. S.					GauU-Scene [144]	24/11	✓	
StreetSurfGS [21]	✓	✓	I		Tem.	✓	✓	✓	✓	✓	G. S.			✓		Free [164]	24/10		
HGS-Mapping [99]	✓	✓	I			✓	✓	✓	✓	✓	G. S.	✓	✓	✓		vKITTI2 [87]	24/03		
GVKF [100]	✓	✓	I			✓	✓	✓		✓	G. S.		✓			Tank and Temple [165], Mip-NeRF 360 [60]	24/11	✓	
DOGS [53]	✓	✓	I		Spa.	✓	✓				G. S.				✓	✓	24/05	✓	
Momentum-GS [48]	✓	✓	I		Spa.	✓					G. S.				✓	✓	24/12	✓	
StreetUnveiler [22]	✓	✓	I	Sem.		✓	✓	✓		✓	G. S.		✓			PandaSet [145]	24/05	✓	

Input-PCL: A—Optional augmentation; S—Supervision; I—Input.

Occl. Idn.: Sem.—Semantic Segmentation; Uncer.—Uncertainty.

Par. Cri.: Spa.—Spatial; Dist.—Distance to Ego; Smpl.—Waypoint Sampling; Tem.—Temporal Chunk.

Open Source: ✓—released to the public; U—unofficial implementation.

TABLE III: Comparison among static and urban scene reconstruction methods.

A. Static Scene Reconstruction

Static scene reconstruction has garnered significant attention due to its unique set of challenges arising from different aspects such as appearance variation, occlusions, and large scale optimization. This section provides an overview of the methods and techniques used in static scene reconstruction, delving into the fundamental elements, including spatial representations, solutions to appearance variation, occlusion identification, and large-scale optimization problem, to offer a holistic understanding of the field. It should be noted that, the content is extended to outdoor reconstruction methods that focus on urban or traffic scenarios considering the commonality of static scene reconstruction.

1) *Representation:* Static scenes are characterized by their large scale, static nature and complex occlusion. Moreover, the input image for large-scale static scenes may come from multiple data collections taken at different times, under different lighting conditions, and with different photometric parameters, termed as appearance variation. Thus, the selection of appropriate primitives becomes crucial for accurate static scene reconstruction.

Methods utilizing implicit representations includes [5], [25], [55], [90], [102], [103]. [5], [55], [102], [103] follow original NeRF, utilize the MLP as primitives while FEGR [5] additionally decomposes spatial representations into three independent components: base geometry, spatially-varying materials for physical-based-rendering, and HDR illumination parameters, achieving improved reconstruction quality with controllable lighting. Inspired by Instant-NGP, [25], [90] adopt multi-

resolution hash grids as their primitive to enable separate modeling of regions at different distance, making optimized trade-off between quality and computational overhead.

Explicit representation-based methods [31], [51], [109], [110] typically integrate highly informative neural representations into computational-efficient explicit representations for improved quality-cost trade-off. Neural Point Light Field [110] encodes light fields on sparse point clouds, enabling efficient view interpolation without requiring dense object coverage or strong input parallax. DGMR [31] develops a dynamic point-based density field derived from NeRF principles, supporting boundary-expandable reconstructions through a specialized multi-scale renderer combining point rasterization with UNet architectures. DNMP [109] evolves traditional meshes into a powerful neural representation by assigning learnable radiance features to deformable mesh vertices. DNMP models local radiance information through the aggregation of vertex features and synthesis novel view with efficient rasterization-based rendering. RoMe [51] reconstructs road surfaces using geometrically and semantically aligned meshes, jointly optimizing learnable vertex attributes containing position, color, semantics and camera poses.

3D Gaussian Splatting [64] introduces a transformative 3D representation with high fidelity and low computational cost, thereby flourishing related researches [2], [3], [30], [89], [92], [99]. [2], [89], [92] use original 3D Gaussians as scene representation. Leveraging salient geometric priors in scenes to regularize the optimization constitutes a intuitive yet effective approach. HGS-Mapping [99] introduces three special-

ized Gaussians for scene modeling: spherical Gaussians with vehicle-aligned rotation for sky modeling, planar 2D Gaussians with fixed normals for road surface, and standard 3D Gaussians for general objects. Similarly, CityGaussianV2 [3] introduces surface-aligned 2D Gaussian supervised by depth estimation from Depth-Anything-V2 [119] and decomposed-gradient-based algorithm for density control to effectively improve surface reconstruction. Moreover, it excludes non-compliant Gaussians from density control to prevent exponential increasing of Gaussians, stabilizing training and reducing artifacts. DHGS [30] incorporates SDF as auxiliary implicit surface representation to regularize the reconstruction of near road.

As a hybrid representation, Gaussian Voxel Kernel Functions (GVKF) [100] unifies the real-time rendering efficiency of 3DGS and continuous surface modeling capabilities of implicit representations, providing a novel alternative for static scene reconstruction. This hybrid framework first constructs a neural opacity field through kernel regression on 3D Gaussian distributions, enabling continuous scene parameterization. It then establishes an explicit neural opacity to SDF conversion module to directly extract surface meshes.

2) *Appearance Variation*: Appearance variation in data collection leads to unstable supervision during training, thus necessitating specialized treatment. Generative Latent Optimization (GLO) [152] has been verified by [89], [90], [92], [102], [103] as a effective solution. Colors are secondarily predicted based on the direct prediction from the model and the appearance embedding from GLO. Appearance embedding captures the dynamic factors and makes the model focusing on learning the invariant features shared across all images. In particular, WildGaussians [92] assigns appearance embedding to each image and each Gaussian to achieve fine-grained optimization. The per-Gaussian embedding is initialized using Fourier Features to enforce local prior. VastGaussian [89] introduces a decoupled appearance modeling framework that first downsamples rendered images, performs pixel-wise concatenation with learnable appearance embeddings, and finally processes the fused features through a CNN to produce transformation maps for adaptive appearance refinement.

3) *Occlusion Identification*: Dynamic occlusions are regarded as noise, thus effective method of identifying and eliminating occlusions from static elements are required. Some approaches [4], [5], [25], [30], [34], [51], [55], [103] directly leverages pre-trained models [6], [10], [13], [14], [16], [121] to provide occlusion semantic masks, while another part of works [49], [92], [102] identify dynamic occlusions as the uncertain regions between images, both of them reduce or ignore the reconstruction loss from the occluded regions during training. NeRF-W [102] adopts an additional transient head to predict color and density distribution in pixel space across image, and derives uncertainty from density covariance. NeRF On-the-go [49] feeds the feature extracted by DINO v2 [120] to a MLP to predict the uncertainty map of a image in latent space. WildGaussians [92] notes that when training with uncertainty supervision, neither MSE used in NeRF-W nor DSSIM in NeRF On-the-go can effectively guide the model to focus on the correct occluders under heavy appearance

changes. To address this problem, WildGaussians proposes DINO cosine similarity as an alternative. This cosine similarity loss based on DINO features is more robust to appearance changes and can better identify occluders during training.

4) *Large-scale Optimization*: Large-scale static scene reconstruction presents significant computational challenge, often surpassing the capacity of individual models or hardware limitations. This challenge has driven a flourishing research of effective partitioning strategies to decompose the massive scenes into manageable sub-units.

Spatial partitioning emerges as an intuitive yet effective strategy, capitalizing on inherent geometric relationships within scene components to guide decomposition processes. Mega-NeRF [4] pioneers spatial partitioning large-scale scenes into multiple blocks which optimized in parallel, and is followed by numerous approaches [2], [89], [103]. Block-NeRF [103] introduces an innovative alignment strategy partitioning scene into overlapping spatial blocks represented by individual MLPs, where the intentional overlap between adjacent blocks enables seamless spatial alignment while maintaining independent optimization. VastGaussian [89] enhances Block-NeRF framework through progressive integration of supervision. Based on camera pose, it partitions scenes into spatial blocks with expanded overlaps for cross-block alignment, then optimizes them by progressively integrating supervisory images and LiDAR data under convergence criteria. Final reconstruction merges non-overlapping Gaussians while discarding buffer-zone redundancies, achieving efficient large-scale modeling. CityGaussian [2] employs a divide-and-conquer approach: pretraining a coarse global 3DGS field with contracting the whole scene into a bounded cubic region, partitioning the cube into spatial regions, then adaptively assigning training data to the region according to a composite criterion: the camera pose is within the region, or the region's improvement to the SSIM loss is significant.

Despite spatial criterion, distance, waypoints of data acquisition, temporal segments of video frames are available options. [30], [90] employ distance as the decoupling criterion. DHGS [30] decouples the scene into near road model and environment model while implementing dedicated optimization schemes for each component. StreetSurf [90] divides the scene into three components according to distance, namely close-range, distant-view and sky and utilizes different models to represent them respectively, cuboid NeuS for close-range, Hyper-cuboid NeRF++ for distant-view and direct MLP for sky. By sampling a manageable waypoint subset and the associated training data each time, RoMe [51] achieves divide-and-conquer processing for large-scale scene reconstruction, completing the overall reconstruction through multiple samplings. StreetSurfGS [21] partitions the input video into multiple intentional overlapped temporal segments for optimizing individually and merging with temporal coherence.

Efficient distributed training methods are equally critical for partitioned blocks. DOGS [53] accelerates large-scale scene reconstruction training by recursively dividing scenes into balanced blocks and optimizing a distributed algorithm with guaranteed convergence. It employs ADMM [122], maintaining a global 3DGS model on the master node for both training

and inference and several local models on worker nodes only used for training. Momentum-GS [48] tackles GPU limitations in large-scale scene reconstruction by using Scene Momentum Self-Distillation with a teacher and multiple student decoders. Student decoders train blocks sequentially and staggered, decoupling block count from GPU availability. A momentum teacher decoder provides a stable reference and consistency loss guides student predictions, whose parameters are updated through a momentum-based formula. Reconstruction-guided block weighting prioritizes under-fitted blocks to balance training and mitigate issues from uneven initial partitioning.

Apart from the partitioning methods, several works have attempted explorations in other directions. CityGaussian [2] additionally incorporate Level-of-Detail (LoD) to address the memory and computation overhead arising from unnecessary Gaussians. Objects in the distance which exhibit fewer details, are represented by a higher-compressed model with LightGaussian [15]. CityGaussianV2 [3] introduces a parallel pipeline that reduces spherical harmonics order and replaces post-pruning in CityGaussian with trimming during block-wise tuning, accelerating training and alleviating memory pressure. HGS-Mapping [99] proposes adaptive update, including silhouette filter, densify control, importance pruning, to enhance reconstruction quality and reduce computational burden by adaptively adding or eliminating Gaussians.

B. Dynamic Object Reconstruction

In autonomous driving scenarios, reconstructing dynamic objects is as crucial as static background reconstruction because dynamic objects, such as vehicles, pedestrians, and cyclists, are key to understanding and predicting the evolving environment. Accurate reconstruction of dynamic objects enables the system to track their movements, anticipate potential collisions, and make safe driving decisions. Sparse observation, heavy occlusion and highly variance are major challenges to dynamic object reconstruction.

Research on vehicle 3D reconstruction remains scarce, with existing efforts predominantly confined to NeRF-based methodologies, while dedicated studies focusing on cyclist reconstruction have yet to emerge. Pedestrian reconstruction is excluded here given its articulated motion complexity, non-rigid surface challenges, and substantial prior advancements in human reconstruction beyond autonomous driving contexts. We refer readers to other human-specific survey [131]–[133] for detailed references.

Car-Studio [137] focus at reconstructing editable cars with NeRF. It proposed a curated dataset CarPatch3D, and a car reconstruction and generation model Car-NeRF. Car-NeRF achieves plausible controllable 3D reconstruction and generation according to single-view observation. The input car image is normalized according to the dimension of the car from the preprocessing module and encoded into texture and shape latent representation with a ResNet-34 pretrained on ImageNet. Cone tracing with integrated positional encoding is adopted rather than ray tracing for continuous scaling and anti-aliasing. DreamCar [47] proposes a synthetic car dataset named Car360 and a composite reconstruction method. It

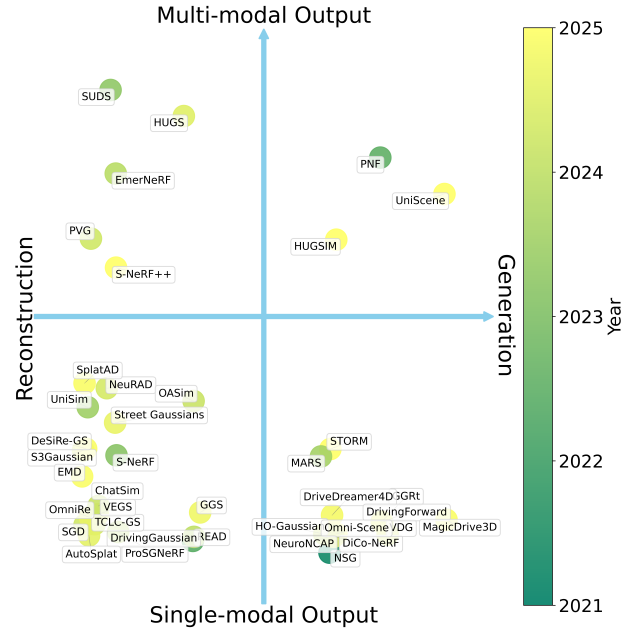


Fig. 3: Illustration of comparison among comprehensive dynamic scene reconstruction methods, generative methods and simulators across methodology paradigm and rendering modality. *Horizontal: Methodology Paradigm; Vertical: Rendering modalities; Color: Release Date.*

employs mirror symmetry to augment limited input views and integrates car-specific generative models via Score Distillation Sampling trained on the proposed Car360 dataset to guide 3D reconstruction under sparse supervision. It combines NeRF, Neus, and DMTET for progressive geometry reconstruction, followed by texture refinement using Stable Diffusion [123] with DreamBooth [124] and LoRA [125], alongside a PoseMLP [126] module to correct dynamic pose errors.

Apart from these standalone reconstruction models, several simulators integrate asset library or sub-modules for high-fidelity vehicle reconstruction [19], [40].

C. Comprehensive Scene Reconstruction

Autonomous driving scenes exhibit inherent complexity, characterized by multi-modal input, multi-scale elements spanning centimeter-level details to distant sky, coupled with dynamic agents (vehicles, pedestrians) coexisting with static structures (buildings, vegetation). This spatial-temporal heterogeneity introduces dual challenges: 1) balancing multi-scale reconstruction fidelity with computational efficiency, and 2) modeling intricate motion patterns and temporal coherence. Current approaches commonly decouple dynamic objects from static backgrounds for independent modeling, enabling adaptive representation design tailored to their distinct spatial-temporal characteristics. In addition, diverse downstream tasks in autonomous driving necessitate the integration of multi-modal data requirements.

In this section, we review recent development in dynamic scene reconstruction with following perspective: input modal-

Method	Task	Input			Decomp.	Repre.	Rendering										Dataset	Release	Open Source	
		Image	Pose	Point Cloud			Image	Depth	Point Cloud	Veh. Pose	Instance	Semantic	Flow	KITTI	vKITTI2	NuScenes				Waymo
																		Others		
NSG [98]	Recon.	✓	✓	-	BBox	NeRF	✓					✓	✓					Argoverse2 [151], ZOD [146]	2021/03	✓
PNF [41]	Recon.	✓	-	-	Self	NeRF	✓	✓		✓	✓		✓				✓		2022/06	
NeuRAD [67]	Recon.	✓	✓	SV.	BBox	NeRF	✓	✓				✓	✓	✓					2024/04	✓
SUDS [88]	Recon.	✓	-	SV.	Self	NeRF	✓	✓		✓	✓	S	✓	✓					2023/03	
EmerNeRF [82]	Recon.	✓	✓	SV.	Self	NeRF	✓	✓	✓			S						NOTR [82]	2023/11	✓
ProSGNeRF [27]	Recon.	✓	✓	SV.	BBox	NeRF	✓	✓					✓	✓					2023/12	S
DiCo-NeRF [66]	Recon.	✓	✓	-	Self	NeRF	✓	✓									✓	JBNU-Depth360 [147]	2024/06	✓
S-NeRF [65]	Recon.	✓	✓	SV.	BBox	NeRF	✓	✓						✓			✓		2023/02	✓
S-NeRF++ [112]	Recon.	✓	✓	SV.	BBox	NeRF	✓	✓			✓	O		✓	✓		✓		2025/01	✓
READ [52]	Recon.	✓	✓	Input	BBox	PCL	✓	✓					✓					Brno Urban [149]	2022/05	✓
DrivingGaussian [111]	Recon.	✓	✓	AUG.	BBox	G. S.	✓	✓						✓			✓		2023/12	✓
GGRI [18]	Recon.	✓	-	-	-	G. S.	✓	✓					✓		✓				2024/03	✓
TCLC-GS [17]	Recon.	✓	✓	Input	-	G. S.	✓	✓							✓	✓			2024/04	
SGD [106]	Recon.	✓	✓	Input	-	G. S.	✓	✓					✓				✓		2024/03	
HO-Gaussian [28]	Recon.	✓	✓	-	-	G. S.	✓	✓								✓		Argoverse2 [151]	2024/03	
S3Gaussian [35]	Recon.	✓	✓	Input	Self	G. S.	✓	✓			✓							NOTR [82]	2024/05	✓
PVG [104]	Recon.	✓	✓	Input	Self	G. S.	✓	✓			✓	V	✓			✓			2024/03	✓
Street Gaussians [34]	Recon.	✓	-	Input	BBox	G. S.	✓	✓	✓				✓	✓					2024/08	✓
OmniRe [115]	Recon.	✓	✓	Input	BBox	G. S.	✓	✓											2024/08	✓
DeSiRe-GS [107]	Recon.	✓	✓	Input	Self	G. S.	✓	✓				V	✓			✓			2024/11	✓
VDG [105]	Recon.	✓	-	-	Self	G. S.	✓	✓					✓			✓			2024/06	S
HUGS [113]	Recon.	✓	✓	Input	BBox	G. S.	✓	✓		✓	✓	O		✓					2024/06	✓
VEGS [32]	Recon.	✓	✓	Input	BBox	G. S.	✓	✓					✓				✓		2024/07	✓
AutoSplat [24]	Recon.	✓	✓	Input	BBox	G. S.	✓	✓					✓					PandaSet [145]	2024/07	
GGs [36]	Recon.	✓	✓	Input	-	G. S.	✓	✓					✓					Brno Urban [149]	2024/09	
DriveDreamer4D [101]	Recon.	✓	✓	-	BBox	G. S.	✓	✓								✓			2024/10	✓
DrivingForward [114]	Recon.	✓	-	-	Self	G. S.	✓	✓											2024/09	
SplatAD [108]	Recon.	✓	✓	Input	BBox	G. S.	✓	✓	✓					✓				Argoverse2 [151], PandaSet [145]	2024/11	S
DreamDrive [118]	Recon.	✓	✓	Input	-	G. S.	✓	✓						✓				Customized	2025/01	
STORM [33]	Recon.	✓	✓	-	Self	G. S.	✓	✓				S	✓			✓		Argoverse2 [151]	2024/12	S
EMD [117]	Recon.	✓	✓	Input	B/S	G. S.	✓	✓				V				✓		NOTR [82]	2024/11	S
Omni-Scene [116]	Recon.	✓	✓	-	-	G. S.	✓	✓						✓					2024/12	✓
UniScene [54]	Gen.	-	-	-	BBox	G. S.	✓	✓	✓		✓			✓					2024/12	S
MagicDrive3D [20]	Gen.	-	-	-	BBox	G.S.	✓	✓	✓										2024/11	S
UniSim [43]	Sim.	✓	✓	Input	BBox	NeRF	✓	✓	✓	✓								PandaSet [145]	2023/06	
MARS [42]	Sim.	✓	✓	-	BBox	NeRF	✓	✓			✓		✓	✓					2023/07	✓
NeuroNCap [1]	Sim.	✓	✓	-	BBox	NeRF	✓	✓	✓					✓					2024/04	✓
OASim [40]	Sim.	✓	✓	AUG.	BBox	NeRF	✓	✓	✓				✓		✓				2024/02	✓
ChatSim [23]	Sim.	✓	✓	Input	BBox	NeRF	✓	✓	✓						✓	✓			2024/02	✓
HUGSIM [19]	Sim.	✓	✓	-	BBox	G.S.	✓	✓	✓		✓	O	✓	✓	✓	✓	✓		2024/12	✓

Task: Recon.—Comprehensive Scene Reconstruction; Gen.—Generation; Sim.—Simulator.

Input-Point Cloud: SV.—Supervision; AUG.—optional augmentation.

Decomp.: BBox—3D Bounding Boxes; Self—Self-supervised; B/S—3D Bounding Boxes or Self-supervised.

Rendering-Flow: S—3D Scene Flow; O—2D Optical Flow; V—Velocity Map.

Repre.: PCL—Point Cloud; G.S.—Gaussian Splatting.

Open Source: ✓—released to the public; S—officially announced but not released yet.

TABLE IV: Overall comparison among comprehensive scene reconstruction, generation methods and simulators.

ity, dynamic-static decomposition methods, representations, rendering modality and methodology paradigm. Figure 3 illustrates comparison among comprehensive scene reconstruction methods, generative methods and simulators across methodology paradigm and rendering modality.

1) *Input Modality:* The input modalities for 3D reconstruction methods originate from mainstream autonomous vehicle sensor suites which typically comprising camera, LiDAR, and GPS/IMU, thereby generally including RGB images, point clouds, and calibration.

Notably, methodological evolution demonstrates a clear trajectory toward reduced sensor modalities, and cost-effective hardware configurations, with increasing emphasis on input robustness under degraded sensing conditions. Based on the information completeness and modality of input data, existing 3D reconstruction methodologies can be taxonomically organized into three levels: multimodal-based reconstruction (fusing heterogeneous sensor data), single modal-based reconstruction (typically depending on image) and generative reconstruction (generating based on indirect conditions).

Multimodal-based reconstruction methods integrate 2D images and 3D point clouds through feature fusion or cross-

modal supervision, establishing a unified 3D representation that synergistically combines photometric details and geometric precision. NeRF-based methods [27], [65], [67], [82], [88], [112] commonly use point cloud as depth supervision by projecting it into imaging plane. Approaches with explicit representation, such as [109], [110] and part of 3DGS-based methods requires LiDAR [24], [32], [34], [35], [104], [107], [108], [115], [117] or SfM pseudo [36], [113], [118] point cloud as input guidance for primitive initialization. SGD [106] innovatively use LiDAR point clouds as the generative condition to improve spatial consistency. DrivingGaussian [111] works without necessarily relying on point cloud data, while being capable to improve reconstruction quality when available.

Single Modal-based methods [18], [28], [33], [41], [66], [98], [101], [116] typically reconstruct with calibrated multi-view 2D input. However, calibration, especially camera extrinsics, are often noisy in driving scenes due to the high-speed movement of mounted vehicle and large-scale scene. VDG [105] estimates and refines relative pose through a pre-trained visual odometry. DrivingForward [114] uses fixed vehicle-to-camera and inter-frame camera motion instead of camera

extrinsics, thereby abandoning expensive video calibration.

Generative methods [20], [54] bypass reliance on explicit image or point cloud inputs, instead utilizing indirect conditioning signals to synthesize virtual scenes with multi-modal rendering outputs, where BEV representations act as efficient semantic priors to guide the scene generation process through spatial-semantic constraints. MagicDrive3D [20] employs multi-modal controls (objects bounding box sequences, BEV maps, ego trajectories, and text prompts) for collaborative scene synthesis, and UniScene [54] generates occupancy fields solely from BEV layouts and subsequently refines it according to text prompt to generate 3D geometry of the synthetic scene.

2) *Representation*: Considering the characteristics of long-range, multi-scale, and the presence of both static and dynamic objects in comprehensive scene, the representation types are broadly varied which can be roughly categorized into three kinds: NeRF-based, point cloud-based, and 3D Gaussian-based, where mesh-based method is underexplored.

NeRF-based Methods Following original NeRF [56], [65]–[67], [98] employ one or multiple MLPs to represent the scene, based on their distinct handling of dynamic and static objects. MLP directly maps every query position to the corresponding radiance field, treating details and texture at different scale with same resolution, making it difficult to trade-off between rendering quality and computational overhead. Utilizing widely appreciated multi-resolution hash grids [12], [61] as spatial representation to encode features, [82], [88], [90], [112] achieve real-time rendering with improved quality. The scene is encoded using multi-resolution hash grids, where each grid stores trainable features. For any query spatial position, the method first retrieves neighboring grid vertices based on spatial proximity, interpolates their features, then processes the weighted features through a lightweight MLP which is substantially smaller thus faster than conventional NeRF decoders to predict radiance fields including density and view-dependent color.

Point Cloud-based Methods Despite the improvement, NeRF-based methods remain constrained by prohibitive computational cost arising from inefficient sampling strategies, limited model capacity, and intricate optimization processes of the implicit representation. READ [52] proposes a novel explicit representation, deriving sparse neural descriptors from point cloud with memory-efficient composite sampling strategies. Each point of the scene is assigned a learnable feature vector that encodes geometry or appearance information. ω -Net is proposed to efficiently reconstruct authentic driving scenes from point cloud subsets sampled via multiple sampling strategies.

3D Gaussian-based Methods Vanilla 3D Gaussian is adopted by [106], [111], [113]–[115], [118] as the scene representation. Despite demonstrating significantly enhanced rendering efficiency and high-fidelity reconstruction quality, 3D Gaussian exhibits limitations including initialization sensitivity, large memory consumption for complex scene and inherent ambiguity for dynamic target.

To provide informative initialization reference for 3D Gaussian, TCLC-GS [17] introduces implicit octree and explicit

meshes derived from images and point clouds, delivering geometric priors with enhanced continuity. HO-Gaussian [28] disentangles view-dependent color from Gaussian primitives and modeled by MLP separately to alleviate memory overhead brought by high-order spherical harmonics. Considering the dynamics in the scene, several works are dedicated to model such time-varying property.

Driving scenarios exhibit inherently high dynamic complexity, necessitating representation capable of precisely modeling intrinsic spatial-temporal features. DreamDrive [118] uses a set of Gaussians to represent the scene at each timestep. DriveDreamer4D [101] incorporates a temporal field which takes origin Gaussian parameters and time as input, predicts offsets with regard to the origin. Periodic Vibration Gaussian (PVG) [104] proposes a novel unified representation for large dynamic urban scene reconstruction. To address the limitations of vanilla 3DGS in representing time-varying dynamic elements, PVG reformulate the mean and opacity of traditional 3D Gaussian into time-dependent functions with learnable life-span, ensuring that for any timestep, the snapshot of the functions still adapt to the pipeline of vanilla 3DGS, and thus can be regarded as a plug-and-play reformulation suitable for any static 3DGS approach. [105], [107], [118] adopt PVG as their dynamic representation. OmniScene [116] introduces a hybrid Gaussian representation integrating voxel-based and pixel-based components, synergistically combines complementary advantages. The voxel-level Gaussians efficiently capture coarse geometric structures with minimal memory consumption, while pixel-aligned Gaussians supplement high-fidelity details beyond voxel boundaries.

3) *Dynamic-static decomposition*: The decoupled reconstruction paradigm originated from Neural Scene Graphs [98], which separates dynamic scenes into independently modeled foreground objects and static backgrounds, has become the standard practice adopted by the majority of subsequent works. NSG [98] employs 3D bounding box annotations to decouple scenes into static nodes for background and dynamic nodes for category-specific objects like vehicles/pedestrians with time-aware 3D bounding boxes, both are represented by MLPs. Within this framework, geometric reconstruction of each dynamic object occurs in canonical coordinates confined by its bounding box. The global scene is then synthesized through spatial transform of bounding boxes into world coordinates for unified rendering. This straightforward scene decomposition paradigm with 3D bounding box annotations has gained wide adoption in subsequent methods [27], [65], [67].

However, the dependency on expensive 3D bounding box annotations for scene decomposition imposes prohibitive costs, fundamentally limiting practical scalability in real-world applications. Some works [35], [66], [82], [104], [105], [107], [113], [114], [118] attempt to eliminate the need for 3D annotations. SUDS [88] and EmerNeRF [82] incorporate static-preferred static-dynamic binary classifications within their density attributes alongside scene flow learning for indirect augmentation. Representations classified as dynamic are assigned time-varying attributes. Furthermore, they take the shadow effect caused by dynamic objects under illumination into account within the decoupling process to prevent unnat-

ural appearance.

Given the geometric consistency of static background across time, many approaches [35], [104], [105], [107], [118] directly adopt time-varying representations for scene modeling, bypassing the preliminary static-dynamic classification. S^3 Gaussian [35] employs spatial-temporal separated Hexplane feature to achieve self-supervised decomposition, with static objects inherently being visible on the three spatial-only planes and dynamic objects are additionally captured on the temporal variation planes. PVG [104] addresses the limitation of vanilla 3DGS in representing time-varying dynamic elements in self-supervised manner, providing a fundamental solution for scene decomposition. Following PVG, [107], [118] are built upon basic time-invariant static model and characterizes the dynamicness by the dissimilarity between the rendered image from the static model and the dynamic ground-truth. VDG [105] enhances PVG by integrating explicit learnable velocity parameters into Gaussian primitives, replacing mean-based implicit velocity estimation of PVG. This velocity field aligns with motion masks from pre-trained visual odometry, enabling precise dynamic region identification.

Several alternative methodologies have proposed distinct solution frameworks to address this challenges. DiCo-NeRF [66] proposes SimLoss regulating the radiance field of NeRF, derived from the cosine similarity maps between the ground-truth and rendered features extracted by CLIP [11] encoder. HUGS [113] employs estimated vehicle pose as an approximation of 3D bounding boxes, simplifying vehicle kinematic with a unicycle model to refine the noisy pose. EMD [117] proposes a plug-and-play motion estimation framework agnostic to both bounding-box-based or self-supervised scene decomposition strategies. It learns cross-temporal correspondence by encoding spatial-temporal Gaussian features through dual-scale deformation networks with positional embeddings, enabling dynamic object trajectory prediction in global coordinates for arbitrary 4D Gaussian reconstruction pipelines.

SGD [106] bypasses explicit decoupling of static backgrounds and dynamic objects with a uniform modeling of the entire scenario. A diffusion model generates geometric and visual consistent novel view conditioning on input image and LiDAR point clouds, which provides pseudo supervision for training 3DGS. While numerous methods [17], [18], [28], [36], [116] focus on addressing other technical challenges, they forgo decoupling mechanisms, imposing uniform modeling across all scene elements directly.

4) *Rendering Modality*: Rendering modalities fundamentally govern the scope of downstream tasks supported by reconstruction methodologies. Contemporary frameworks increasingly adopt multi-modal rendering paradigms to holistically replicate well-annotated field-acquired dataset with physically-grounded sensor response characteristics and diverse fine-grained annotations.

Image As the most fundamental modality in 3D reconstruction, 2D images constitute an indispensable component across all methodological approaches. Notably, DiCo-NeRF [66] stands out as one of the few works implementing fisheye-view rendering, providing critical support for specific perception systems and solutions. This innovation directly addresses the

demands of perception systems requiring panoramic environmental awareness, where conventional pinhole camera models fail to capture seamless peripheral details.

Depth Map Most methodologies [17], [18], [27], [32]–[36], [41], [65], [67], [82], [88], [101], [104]–[108], [112]–[116] employ depth maps as 2D geometric proxies for spatial information, where 3D scene geometry is projected onto the 2D imaging plane via perspective transformation. While depth maps retain partial spatial cues (e.g., relative distances), they inherently incur lossy spatial encoding due to dimension reduction, discarding critical 3D structural details (e.g., surface normals, multi-view consistency) and introducing ambiguity in occluded regions.

Point Cloud The widespread adoption of LiDAR in autonomous driving vehicles emphasize the importance of spatial-coherent point clouds synthesis in reconstruction to keep faithful reflection of field-acquired sensor data. Due to the uniqueness of the imaging method, LiDAR point clouds have distinct characteristics from 2D images. [67], [108] consider ray drop probability indicating the chance that a LiDAR ray does not return and rolling shutter effects which account for the distortion arise from the sequential capture of scenes by LiDAR scan and rapid movement of vehicle, thereby enabling more realistic multi-modal simulations. EmerNeRF [82] simulate LiDAR sampling in asynchronized manner with a combined supervision of expected depth and line-of-sight constraints, enforcing unimodal density distributions along sampling ray, which is critical for disambiguating static-dynamic scene elements through volumetric rendering. Splatad [108] develops a projection algorithm in spherical coordinate and customizes a tiling, sorting, and rasterization pipeline tailored for imitating the imaging process of LiDAR, which achieves superior efficiency and realism.

Annotations Despite perceptual modalities, annotation plays a crucial role in modern autonomous driving system for identifying and tracking environmental elements. PNF [41] represents a pioneering extension of NeRF to semantic radiance fields, augmenting rendered outputs with instance segmentation alongside photorealistic RGB and depth, supporting diverse downstream perception tasks. [34], [35], [88], [104], [112], [113] provide semantic segmentation results, and [88], [113] follows PNF to additionally incorporate instance segmentation annotations.

Vehicle pose estimation, which provides relative positional relationships between surrounding vehicles and the ego-vehicle, constitutes a critical component in scene understanding, with common formats including 3D bounding boxes and waypoints. While conventional approaches require pose as explicit input, emerging methods not only eliminate this dependency but also actively estimate pose during 3D reconstruction. SUDS [88] derives bounding boxes via PCA from instance segmentation results of 3D point cloud, while [34], [41] optimizes parameterized pose within their training frameworks.

Flow field, including optical flow and scene flow, captures dynamic motion patterns and enhances spatial-temporal coherence. Several frameworks incorporate flow learning to not only generate pseudo supervision for downstream tasks, such

as vehicle detection or motion prediction, but also enhance reconstruction and novel view synthesis quality. SUDS [88] leverages pre-trained DINO to extract 2D optical flow, which serves as supervisory information for learning 3D scene flow. As a completely self-supervised approach, EmerNeRF [82] optimize flow estimation through indirectly reconstruction loss according to the hypothesis that only temporally-consistent features benefit from multi-frame feature integration, and further justify the hypothesis in ablation study. [65], [112] integrate optical flow as both a cross-view geometric consistency regularization and confidence basis, effectively mitigating aliasing artifacts. In the realm of 3DGS, there exists an explicit and mathematically grounded correlation between flow and the center of Gaussians. This bidirectional relationship enables mutual deriving flow from Gaussian movement [113] and vice versa [33], thereby facilitating joint optimization that simultaneously enhances motion coherence and geometric fidelity through gradient-based coupling. The reformulation of Gaussians in PVG [104], [105], [107] incorporates an additional velocity attribute, which can be interpreted as. Velocity can be interpreted as a variant of flow fields that explicitly characterizes the temporal evolution of the scene, which can be inferred from time-varying Gaussian primitives [104], [107], [118] or directly learnt [105], [117].

5) *Methodology Paradigm*: Common methods [18], [41], [52], [67], [98], [111], [115] follow per-scene reconstruction paradigm requiring sufficient ground truth observation from diverse viewpoints, which inherently suffers from heavy data acquisition cost and limited generalization capability. Consequently, the practical deployment of these methods becomes fundamentally constrained. DrivingForward [114] proposes a generalizable feed-forward approach to achieve real-time driving scene reconstruction at inference. Specifically, the parameters of 3D Gaussians are predicted based on the input video, which greatly enhances the generalization ability for novel scenes.

The rapid advancement of generative models, particularly diffusion-based architectures, is driving a paradigm shift in 3D reconstruction with an increasing number of approaches transitioning toward generative frameworks. While video generation models offer supplementary supervision for 3D reconstruction, their inherent 2D training paradigm fundamentally lacks 3D spatial awareness, inevitably introducing unrealistic artifacts and spatial discontinuities that degrade reconstruction fidelity. [101], [118] provide distinct solution to effectively integrate 2D video generation models into 3D reconstruction. To improve generalization ability to novel views, DriveDreamer4D [101] synthesis counterfactual videos according to modified ego trajectories and structural information, then constructs temporally aligned cousin-pair data through synchronized composition of synthetic and original sequences for training. It leverages L1-distance between the feature map of synthetic and original videos as regularization to effectively ensure spatial consistent to real world. DreamDrive [118] enhances spatial-temporal modeling accuracy of 4D Gaussian with video generative model. The framework first conditions video diffusion models on real-world information to generate supplementary novel view observations, which inherently

contain fake spatial dynamics. To mitigate this, it leverages the motion consistency across local parts of a rigid-body to perform clustering and smoothing on Gaussians belonging to the same object, thereby filtering out fake dynamics.

Furthermore, generative methodologies can transcend the constraints of 2D planar representations by enabling direct generation in 3D space, as will be discussed in Section IV-D.

D. Applications

1) *Scene Generation*: 3D generative methods are critical in autonomous driving for scalable scenario synthesis, reducing reliance on resource-intensive data acquisition and mitigating safety risks associated with collecting rare-edge cases (e.g., extreme weather, collision scenarios) essential for addressing long-tail challenges. Guided by high-level informative conditions like BEV map and text prompt, these approaches efficiently produce diverse driving scenes at minimal cost.

MagicDrive3D [20] achieves controllable 3D scene generation through multi-modal guidance including bounding boxes and BEV map. It first synthesizes temporal consistent multi-view videos controlled by guidance, then geometrically lifts them to 3D point cloud via pre-trained monocular depth model and unprojection. This point cloud serves as initialization prior of deformable Gaussians for spatial-temporally coherent reconstruction, addressing both geometric fidelity and motion consistency in generation.

UniScene [54] takes BEV layouts as input, utilizing occupancy grids as central spatial representation to produce aligned multimodal camera-LiDAR outputs. The framework first elevates 2D BEV layout frames into a time-varying 3D semantic occupancy grid through a diffusion transformer, creating a unified spatial foundation for camera video and LiDAR point cloud generation while ensuring temporal coherence by inherent cross-frame consistency within BEV frames. The video generation pipeline employs Gaussian splatting to transform occupancy grids into semantic and depth maps, which are subsequently integrated with supplementary text prompts to synthesize photorealistic video sequences via stable diffusion. Meanwhile, LiDAR point clouds are obtained by sampling the occupancy representation in voxel space, preserving geometric consistency across modalities.

For static background, while urban scene generative methods [93]–[97] demonstrate potential for static driving environment generation, they exhibit low rendering quality with insufficient detail and realism, expecting further exploration in future research endeavors.

2) *Simulator*: Simulator plays a crucial role in autonomous driving for reduction of time, cost and safety risk. Conventional game-engine based simulator mostly require manual design of scenes and 3D models, which results in a significant discrepancy between the generated perceptual distribution and that of the real world. Such difference offers opportunities for simulators based on 3D reconstruction, as they can provide more realistic perceptual data distributions. Evolved from comprehensive scene reconstruction frameworks, reconstruction based simulators achieve fine-grained environment con-

trol through decomposing scenes into static backgrounds and dynamic foregrounds with separate modeling.

UniSim [43] employs NeRF for closed-loop multi-sensor simulator using driving logs, the static environment is represented through a multi-resolution feature grid with MLP decoding, where LiDAR-derived geometry priors sparsify grids by optimizing near-surface voxel features. Dynamic actors utilize shared HyperNet-generated feature grids conditioned on latent codes, capturing visibility correlations through learned generalized priors. Joint camera-LiDAR supervision enables multimodal simulation, particularly enhancing novel view synthesis in large-scale extrapolation scenarios.

MARS [42] is a highly configurable simulator platform that supports switching between diverse NeRF variants as backend renderer, multiple ray sampling strategies, and multimodal inputs, while providing RGB, depth, and semantic rendering outputs. As the first open-source, configurable NeRF-based simulator for both academic and industrial communities, MARS provides a valuable reference for subsequent development of reconstruction-based simulators.

OASim [40] provides a dynamic object asset library comprising diverse vehicle models to enable high-fidelity novel view synthesis, particularly under significant viewpoint variations relative to dynamic objects. Additionally, the framework is equipped with an user-friendly graphical interface for configuring simulator, including fine-grained traffic participant trajectory customization and multi-sensor perception setup.

HUGSIM [19] extends HUGS as a closed-loop simulator, establishing the first 3DGS-based Simulator framework. It outperforms NeRF-based methods with significantly accelerated rendering speeds while supporting diverse rendering modalities. HUGSIM integrates an trajectory generator to eliminate manual vehicle trajectory design and incorporates a vehicle asset library reconstructed from 3DRealCar to enhance rendering fidelity. Additionally, it proposes a comprehensive benchmark for simulators and conducts comparative analyses of closed-loop simulation paradigms, offering methodological support for future simulator development.

3) *Scene Understanding*: Several methods do not implement systematic improvements to reconstruction techniques, but instead achieve novel integration into autonomous driving systems through innovative model architecture design or training paradigm optimization, which significantly enhances environmental perception and scene understanding capabilities.

PreSight [127] introduces a novel framework that leverages historical traversal data to construct static prior memories using NeRF. These priors, which are rich in semantic and geometric details, are derived without manual annotations and can improve the performance of various state-of-the-art perception models with slight additional computational cost. Specifically, a city-scale NeRF is constructed with the historical observation and encoded into BEV or 3D prior features by voxelization and processing with convolutional network. Such prior features can be easily fused into online features as a augmentation with rich environmental information.

UniPAD [128] innovatively integrates 3D reconstruction to address partial observation in driving scenarios, achieving sub-

stantial enhancement in scene perception and understanding. Given partial observed point clouds and images of the environment, the framework synergizes masked autoencoders with 3D differentiable volume rendering, embedding geometric completion directly into the training pipeline. This reconstruction-enhanced paradigm delivers enriched scene geometry to downstream perception modules, yielding remarkable performance gains across multiple tasks including object tracking and 3D semantic segmentation.

GaussianAD [129] introduces a vision-centric end-to-end autonomous driving framework utilizing 3D Gaussians as explicit scene representations. It employs 3D Gaussians as the core scene representation for understanding and downstream tasks, ranging from dense tasks like 3D semantic occupancy prediction to sparse task, such as object detection and motion prediction. Moreover, Gaussian Flow is formally defined as the motion vector field of 3D Gaussians within a scene, which is jointly predicted through the synergistic integration of neural scene representations and ego-motion trajectory estimation. Gaussian Flow establishes a comprehensive and robust foundation for spatial-temporal forecasting in dynamic environments, enabling efficient computation of future scene representation with affine transformation.

RAD [130] innovatively integrates closed-loop simulation grounded in 3D reconstruction into reinforcement learning frameworks, establishing a post-training paradigm that enables continuous policy refinement through photorealistic environment interactions. The RAD planner strategically integrates dual policy heads with complementary roles: The imitation learning (IL) component, trained on expert demonstrations, stabilizes action distribution initialization and enforces behavioral regularization for the reinforcement learning counterpart. Conversely, the reinforcement learning (RL) head proactively explores beyond demonstrated strategies, overcoming the inherent performance constraints of imitation-based approaches to address novel out-of-distribution scenarios. RAD integrates a 3DGS-based closed-loop simulator for reinforced post-training the RL head. This simulator identifies high-risk scenarios, reconstructs the environment and traffic participants via 3DGS, and evolves these scenarios in log-replay manner. Within this synthetic environment, the planner is iteratively optimized with regard to the reward offered by the simulator, thereby achieving progressive performance enhancement through adversarial interaction with dynamically generated edge cases.

V. OUTLOOK & CHALLENGES

As discussed in Section IV, 3D reconstruction in autonomous driving has evolved across multiple dimensions, including technical paradigm, spatial representations, and task-specific integration levels, yet persistent challenges remain unresolved for future research.

Technical paradigm A paradigm evolution from reconstructive to generative approaches is evident in comprehensive scene and static background reconstruction, driven by the reduced input dependencies transitioning from aligned multimodal annotated data [26], [34], [67], [89] to standalone

BEV maps [54], as well as the training strategy shift from per-scene training models [41], [82], [98] and feedforward prediction networks [114] to ultimately generalizable generative models [20], [54]. This evolution provides new opportunity for 3D reconstruction, enabling potential integration with high-level informative condition to construct large-scale world models capable of autonomous 3D space generation, thereby expanding explorable spatial-semantic environments. Moreover, diverse informative conditions such as

Spatial Representations Spatial representations have evolved from compact yet sample-inefficient implicit models and real-time rendering yet information-sparse explicit methods toward compact neural explicit representations. While this transition significantly improves training/render efficiency, it struggles with geometric inaccuracies arising from discretization. Emerging hybrid approaches integrate implicit geometric completeness with explicit rendering efficiency [100], [161]–[163], yet dynamic scene modeling remains unexplored. Autonomous driving urges unified spatial-temporal representations that jointly preserve geometric fidelity, computational tractability, and spatial-temporal consistency especially for dynamic objects and high-speed viewpoint change.

Integration Level Early approaches treated 3D reconstruction primarily as a tool for data augmentation and modality completion, focusing on sensor data fidelity. Subsequent methods integrated reconstruction into closed-loop simulation platforms with controllable agent behaviors, enabling counterfactual scenario simulation to support algorithm training and validation. Recent advancements further integrating 3D reconstruction as scene understanding modules with autonomous driving models, progressively transforming it from auxiliary preprocessing to core perception-modelling co-design. 3D reconstruction techniques approximate complete spatial information from partially observed sensor data, providing autonomous driving systems with robust geometric priors and creating potential for deeper, more innovative integration in future autonomous driving developments.

VI. CONCLUSION

While learning-based 3D reconstruction introduces transformative techniques for autonomous systems, critical challenges persist in various perspectives such as scalability, dynamic scene modeling, and real-time constraints. This survey provides a systematic review of learning-based 3D reconstruction in autonomous driving, spanning data, methodological advancements, and emerging trends. Organized hierarchically from fundamentals to cutting-edge techniques, this review serves both researchers and practitioners with actionable insights and references. We hope this survey could inspire future innovations.

REFERENCES

- [1] W. Ljungbergh, A. Tonderski, J. Johnander, H. Caesar, K. Åström, M. Felsberg, and C. Petersson, “Neuroncap: Photorealistic closed-loop safety testing for autonomous driving,” in *European Conference on Computer Vision*. Springer, 2024, pp. 161–177.
- [2] Y. Liu, C. Luo, L. Fan, N. Wang, J. Peng, and Z. Zhang, “Citygaussian: Real-time high-quality large-scale scene rendering with gaussians,” in *European Conference on Computer Vision*. Springer, 2024, pp. 265–282.
- [3] Y. Liu, C. Luo, Z. Mao, J. Peng, and Z. Zhang, “Citygaussianv2: Efficient and geometrically accurate reconstruction for large-scale scenes,” *arXiv preprint arXiv:2411.00771*, 2024.
- [4] H. Turki, D. Ramanan, and M. Satyanarayanan, “Mega-nerf: Scalable construction of large-scale nerfs for virtual fly-throughs,” in *Proceedings of the IEEE/CVF conference on computer vision and pattern recognition*, 2022, pp. 12 922–12 931.
- [5] Z. Wang, T. Shen, J. Gao, S. Huang, J. Munkberg, J. Hasselgren, Z. Gojcic, W. Chen, and S. Fidler, “Neural fields meet explicit geometric representations for inverse rendering of urban scenes,” in *Proceedings of the IEEE/CVF Conference on Computer Vision and Pattern Recognition*, 2023, pp. 8370–8380.
- [6] A. Tao, K. Sapra, and B. Catanzaro, “Hierarchical multi-scale attention for semantic segmentation,” *arXiv preprint arXiv:2005.10821*, 2020.
- [7] C. Szegedy, V. Vanhoucke, S. Ioffe, J. Shlens, and Z. Wojna, “Rethinking the inception architecture for computer vision,” in *Proceedings of the IEEE conference on computer vision and pattern recognition*, 2016, pp. 2818–2826.
- [8] K. Simonyan and A. Zisserman, “Very deep convolutional networks for large-scale image recognition,” *arXiv preprint arXiv:1409.1556*, 2014.
- [9] A. Krizhevsky, I. Sutskever, and G. E. Hinton, “Imagenet classification with deep convolutional neural networks,” *Advances in neural information processing systems*, vol. 25, 2012.
- [10] L.-C. Chen, G. Papandreou, F. Schroff, and H. Adam, “Rethinking atrous convolution for semantic image segmentation,” *arXiv preprint arXiv:1706.05587*, 2017.
- [11] A. Radford, J. W. Kim, C. Hallacy, A. Ramesh, G. Goh, S. Agarwal, G. Sastry, A. Askell, P. Mishkin, J. Clark *et al.*, “Learning transferable visual models from natural language supervision,” in *International conference on machine learning*. PmlR, 2021, pp. 8748–8763.
- [12] J. T. Barron, B. Mildenhall, D. Verbin, P. P. Srinivasan, and P. Hedman, “Zip-nerf: Anti-aliased grid-based neural radiance fields,” in *Proceedings of the IEEE/CVF International Conference on Computer Vision (ICCV)*, October 2023, pp. 19 697–19 705.
- [13] L.-C. Chen, Y. Zhu, G. Papandreou, F. Schroff, and H. Adam, “Encoder-decoder with atrous separable convolution for semantic image segmentation,” in *Proceedings of the European conference on computer vision (ECCV)*, 2018, pp. 801–818.
- [14] B. Cheng, M. D. Collins, Y. Zhu, T. Liu, T. S. Huang, H. Adam, and L.-C. Chen, “Panoptic-deeplab: A simple, strong, and fast baseline for bottom-up panoptic segmentation,” in *Proceedings of the IEEE/CVF conference on computer vision and pattern recognition*, 2020, pp. 12 475–12 485.
- [15] Z. Fan, K. Wang, K. Wen, Z. Zhu, D. Xu, Z. Wang *et al.*, “Lightgaussian: Unbounded 3d gaussian compression with 15x reduction and 200+ fps,” *Advances in neural information processing systems*, vol. 37, pp. 140 138–140 158, 2024.
- [16] E. Xie, W. Wang, Z. Yu, A. Anandkumar, J. M. Alvarez, and P. Luo, “Segformer: Simple and efficient design for semantic segmentation with transformers,” *Advances in neural information processing systems*, vol. 34, pp. 12 077–12 090, 2021.
- [17] C. Zhao, S. Sun, R. Wang, Y. Guo, J.-J. Wan, Z. Huang, X. Huang, Y. V. Chen, and L. Ren, “Tclc-gs: Tightly coupled lidar-camera gaussian splatting for autonomous driving: Supplementary materials,” in *European Conference on Computer Vision*. Springer, 2024, pp. 91–106.
- [18] H. Li, Y. Gao, C. Wu, D. Zhang, Y. Dai, C. Zhao, H. Feng, E. Ding, J. Wang, and J. Han, “Ggrt: Towards pose-free generalizable 3d gaussian splatting in real-time,” in *European Conference on Computer Vision*. Springer, 2024, pp. 325–341.
- [19] H. Zhou, L. Lin, J. Wang, Y. Lu, D. Bai, B. Liu, Y. Wang, A. Geiger, and Y. Liao, “Hugsim: A real-time, photo-realistic and closed-loop simulator for autonomous driving,” *arXiv preprint arXiv:2412.01718*, 2024.
- [20] R. Gao, K. Chen, Z. Li, L. Hong, Z. Li, and Q. Xu, “Magicdrive3d: Controllable 3d generation for any-view rendering in street scenes,” *arXiv preprint arXiv:2405.14475*, 2024.
- [21] X. Cui, W. Ye, Y. Wang, G. Zhang, W. Zhou, and H. Li, “Streetsurfgs: Scalable urban street surface reconstruction with planar-based gaussian splatting,” *arXiv preprint arXiv:2410.04354*, 2024.
- [22] J. Xu, Y. Wang, Y. Zhao, Y. Fu, and S. Gao, “3d streetunveiler with semantic-aware 2dgs,” *arXiv preprint arXiv:2405.18416*, 2024.
- [23] Y. Wei, Z. Wang, Y. Lu, C. Xu, C. Liu, H. Zhao, S. Chen, and Y. Wang, “Editable scene simulation for autonomous driving via collaborative llm-agents,” in *Proceedings of the IEEE/CVF Conference on Computer Vision and Pattern Recognition*, 2024, pp. 15 077–15 087.
- [24] M. Khan, H. Fazlali, D. Sharma, T. Cao, D. Bai, Y. Ren, and B. Liu, “Autosplat: Constrained gaussian splatting for autonomous driving scene reconstruction,” *arXiv preprint arXiv:2407.02598*, 2024.

- [25] F. Wang, A. Louys, N. Piasco, M. Bennehar, L. Roldão, and D. Tsishkou, "Planerf: Svd unsupervised 3d plane regularization for nerf large-scale scene reconstruction," *arXiv preprint arXiv:2305.16914*, 2023.
- [26] T. Tao, G. Wang, Y. Lao, P. Chen, J. Liu, L. Lin, K. Yu, and X. Liang, "Alignmf: Geometry-aligned multimodal implicit field for lidar-camera joint synthesis," in *Proceedings of the IEEE/CVF Conference on Computer Vision and Pattern Recognition*, 2024, pp. 21 230–21 240.
- [27] T. Deng, S. Liu, X. Wang, Y. Liu, D. Wang, and W. Chen, "Prosgnerf: Progressive dynamic neural scene graph with frequency modulated auto-encoder in urban scenes," *arXiv preprint arXiv:2312.09076*, 2023.
- [28] Z. Li, Y. Zhang, C. Wu, J. Zhu, and L. Zhang, "Ho-gaussian: Hybrid optimization of 3d gaussian splatting for urban scenes," in *European Conference on Computer Vision*. Springer, 2024, pp. 19–36.
- [29] Q. Chen, S. Yang, S. Du, T. Tang, P. Chen, and Y. Huo, "Lidar-gs: Real-time lidar re-simulation using gaussian splatting," *arXiv preprint arXiv:2410.05111*, 2024.
- [30] X. Shi, L. Chen, P. Wei, X. Wu, T. Jiang, Y. Luo, and L. Xie, "Dhgs: Decoupled hybrid gaussian splatting for driving scene," *arXiv preprint arXiv:2407.16600*, 2024.
- [31] Z. Li, C. Wu, L. Zhang, and J. Zhu, "Dgnr: Density-guided neural point rendering of large driving scenes," *IEEE Transactions on Automation Science and Engineering*, 2024.
- [32] S. Hwang, M.-J. Kim, T. Kang, J. Kang, and J. Choo, "Vegs: View extrapolation of urban scenes in 3d gaussian splatting using learned priors," in *European Conference on Computer Vision*. Springer, 2024, pp. 1–18.
- [33] J. Yang, J. Huang, Y. Chen, Y. Wang, B. Li, Y. You, A. Sharma, M. Igl, P. Karkus, D. Xu *et al.*, "Storm: Spatio-temporal reconstruction model for large-scale outdoor scenes," *arXiv preprint arXiv:2501.00602*, 2024.
- [34] Y. Yan, H. Lin, C. Zhou, W. Wang, H. Sun, K. Zhan, X. Lang, X. Zhou, and S. Peng, "Street gaussians: Modeling dynamic urban scenes with gaussian splatting," in *European Conference on Computer Vision*. Springer, 2024, pp. 156–173.
- [35] N. Huang, X. Wei, W. Zheng, P. An, M. Lu, W. Zhan, M. Tomizuka, K. Keutzer, and S. Zhang, "S³ gaussian: Self-supervised street gaussians for autonomous driving," *arXiv preprint arXiv:2405.20323*, 2024.
- [36] H. Han, K. Zhou, X. Long, Y. Wang, and C. Xiao, "Ggs: Generalizable gaussian splatting for lane switching in autonomous driving," *arXiv preprint arXiv:2409.02382*, 2024.
- [37] H. Li, M. Yuan, Y. Zhang, C. Wu, C. Zhao, C. Song, H. Feng, E. Ding, D. Zhang, and J. Wang, "Xld: a cross-lane dataset for benchmarking novel driving view synthesis," *arXiv preprint arXiv:2406.18360*, 2024.
- [38] L. Li, H. Feng, and J. Xin, "A controllable editing closed-loop 3d gaussian autonomous driving sensor simulator," in *2024 China Automation Congress (CAC)*. IEEE, 2024, pp. 3252–3256.
- [39] T. Yan, D. Wu, W. Han, J. Jiang, X. Zhou, K. Zhan, C.-z. Xu, and J. Shen, "Drivingsphere: Building a high-fidelity 4d world for closed-loop simulation," *arXiv preprint arXiv:2411.11252*, 2024.
- [40] G. Yan, J. Pi, J. Guo, Z. Luo, M. Dou, N. Deng, Q. Huang, D. Fu, L. Wen, P. Cai *et al.*, "Oasim: An open and adaptive simulator based on neural rendering for autonomous driving," *arXiv preprint arXiv:2402.03830*, 2024.
- [41] A. Kundu, K. Genova, X. Yin, A. Fathi, C. Pantofaru, L. J. Guibas, A. Tagliasacchi, F. Dellaert, and T. Funkhouser, "Panoptic neural fields: A semantic object-aware neural scene representation," in *Proceedings of the IEEE/CVF Conference on Computer Vision and Pattern Recognition*, 2022, pp. 12 871–12 881.
- [42] Z. Wu, T. Liu, L. Luo, Z. Zhong, J. Chen, H. Xiao, C. Hou, H. Lou, Y. Chen, R. Yang *et al.*, "Mars: An instance-aware, modular and realistic simulator for autonomous driving," in *CAAI International Conference on Artificial Intelligence*. Springer, 2023, pp. 3–15.
- [43] Z. Yang, Y. Chen, J. Wang, S. Manivasagam, W.-C. Ma, A. J. Yang, and R. Urtasun, "Unisim: A neural closed-loop sensor simulator," in *Proceedings of the IEEE/CVF Conference on Computer Vision and Pattern Recognition*, 2023, pp. 1389–1399.
- [44] T. Lu, M. Yu, L. Xu, Y. Xiangli, L. Wang, D. Lin, and B. Dai, "Scaffold-gs: Structured 3d gaussians for view-adaptive rendering," in *Proceedings of the IEEE/CVF Conference on Computer Vision and Pattern Recognition*, 2024, pp. 20 654–20 664.
- [45] Z. Yu, A. Chen, B. Huang, T. Sattler, and A. Geiger, "Mip-splatting: Alias-free 3d gaussian splatting," in *Proceedings of the IEEE/CVF conference on computer vision and pattern recognition*, 2024, pp. 19 447–19 456.
- [46] X. Du, H. Sun, S. Wang, Z. Wu, H. Sheng, J. Ying, M. Lu, T. Zhu, K. Zhan, and X. Yu, "3drealcar: An in-the-wild rgb-d car dataset with 360-degree views," *arXiv preprint arXiv:2406.04875*, 2024.
- [47] X. Du, H. Sun, M. Lu, T. Zhu, and X. Yu, "Dreamcar: Leveraging car-specific prior for in-the-wild 3d car reconstruction," *IEEE Robotics and Automation Letters*, 2024.
- [48] J. Fan, W. Li, Y. Han, and Y. Tang, "Momentum-gs: Momentum gaussian self-distillation for high-quality large scene reconstruction," *arXiv preprint arXiv:2412.04887*, 2024.
- [49] W. Ren, Z. Zhu, B. Sun, J. Chen, M. Pollefeys, and S. Peng, "Nerf on-the-go: Exploiting uncertainty for distractor-free nerfs in the wild," in *Proceedings of the IEEE/CVF Conference on Computer Vision and Pattern Recognition*, 2024, pp. 8931–8940.
- [50] S. Sabour, S. Vora, D. Duckworth, I. Krasin, D. J. Fleet, and A. Tagliasacchi, "Robustnerf: Ignoring distractors with robust losses," in *Proceedings of the IEEE/CVF conference on computer vision and pattern recognition*, 2023, pp. 20 626–20 636.
- [51] R. Mei, W. Sui, J. Zhang, X. Qin, G. Wang, T. Peng, T. Chen, and C. Yang, "Rome: Towards large scale road surface reconstruction via mesh representation," *IEEE Transactions on Intelligent Vehicles*, 2024.
- [52] Z. Li, L. Li, and J. Zhu, "Read: Large-scale neural scene rendering for autonomous driving," in *Proceedings of the AAAI Conference on Artificial Intelligence*, vol. 37, no. 2, 2023, pp. 1522–1529.
- [53] Y. Chen and G. H. Lee, "Dogs: Distributed-oriented gaussian splatting for large-scale 3d reconstruction via gaussian consensus," *Advances in Neural Information Processing Systems*, vol. 37, pp. 34 487–34 512, 2024.
- [54] B. Li, J. Guo, H. Liu, Y. Zou, Y. Ding, X. Chen, H. Zhu, F. Tan, C. Zhang, T. Wang *et al.*, "Uniscene: Unified occupancy-centric driving scene generation," *arXiv preprint arXiv:2412.05435*, 2024.
- [55] K. Rematas, A. Liu, P. P. Srinivasan, J. T. Barron, A. Tagliasacchi, T. Funkhouser, and V. Ferrari, "Urban radiance fields," in *Proceedings of the IEEE/CVF Conference on Computer Vision and Pattern Recognition*, 2022, pp. 12 932–12 942.
- [56] B. Mildenhall, P. P. Srinivasan, M. Tancik, J. T. Barron, R. Ramamoorthi, and R. Ng, "Nerf: Representing scenes as neural radiance fields for view synthesis," *Communications of the ACM*, vol. 65, no. 1, pp. 99–106, 2021.
- [57] K. Zhang, G. Riegler, N. Snavely, and V. Koltun, "Nerf++: Analyzing and improving neural radiance fields," *arXiv preprint arXiv:2010.07492*, 2020.
- [58] P. Wang, L. Liu, Y. Liu, C. Theobalt, T. Komura, and W. Wang, "Neus: Learning neural implicit surfaces by volume rendering for multi-view reconstruction," *ArXiv*, vol. abs/2106.10689, 2021.
- [59] J. T. Barron, B. Mildenhall, M. Tancik, P. Hedman, R. Martin-Brualla, and P. P. Srinivasan, "Mip-nerf: A multiscale representation for anti-aliasing neural radiance fields," *2021 IEEE/CVF International Conference on Computer Vision (ICCV)*, pp. 5835–5844, 2021.
- [60] J. T. Barron, B. Mildenhall, D. Verbin, P. P. Srinivasan, and P. Hedman, "Mip-nerf 360: Unbounded anti-aliased neural radiance fields," *2022 IEEE/CVF Conference on Computer Vision and Pattern Recognition (CVPR)*, pp. 5460–5469, 2021.
- [61] T. Müller, A. Evans, C. Schied, and A. Keller, "Instant neural graphics primitives with a multiresolution hash encoding," *ACM Transactions on Graphics (TOG)*, vol. 41, pp. 1 – 15, 2022.
- [62] S. Szymanowicz, C. Rupprecht, and A. Vedaldi, "Splatter image: Ultra-fast single-view 3d reconstruction," *2024 IEEE/CVF Conference on Computer Vision and Pattern Recognition (CVPR)*, pp. 10 208–10 217, 2023.
- [63] J. Tang, Z. Chen, X. Chen, T. Wang, G. Zeng, and Z. Liu, "Lgm: Large multi-view gaussian model for high-resolution 3d content creation," in *European Conference on Computer Vision*, 2024.
- [64] B. Kerbl, G. Kopanas, T. Leimkühler, and G. Drettakis, "3d gaussian splatting for real-time radiance field rendering," *ACM Trans. Graph.*, vol. 42, no. 4, pp. 139–1, 2023.
- [65] Z. Xie, J. Zhang, W. Li, F. Zhang, and L. Zhang, "S-nerf: Neural radiance fields for street views," *arXiv preprint arXiv:2303.00749*, 2023.
- [66] J. Choi, G. Hwang, and S. J. Lee, "Dico-nerf: Difference of cosine similarity for neural rendering of fisheye driving scenes," in *Proceedings of the IEEE/CVF Conference on Computer Vision and Pattern Recognition*, 2024, pp. 7850–7858.
- [67] A. Tonderski, C. Lindström, G. Hess, W. Ljungbergh, L. Svensson, and C. Petersson, "Neurad: Neural rendering for autonomous driving," in *Proceedings of the IEEE/CVF Conference on Computer Vision and Pattern Recognition*, 2024, pp. 14 895–14 904.
- [68] Q. Wang, L. Fan, Y. Wang, Y. Chen, and Z. Zhang, "Freevs: Generative view synthesis on free driving trajectory," *arXiv preprint arXiv:2410.18079*, 2024.
- [69] Y. Wang, J. He, L. Fan, H. Li, Y. Chen, and Z. Zhang, "Driving into the future: Multiview visual forecasting and planning with world model

- for autonomous driving,” in *Proceedings of the IEEE/CVF Conference on Computer Vision and Pattern Recognition*, 2024, pp. 14 749–14 759.
- [70] J. Lu, Z. Huang, Z. Yang, J. Zhang, and L. Zhang, “Wovogen: World volume-aware diffusion for controllable multi-camera driving scene generation,” in *European Conference on Computer Vision*. Springer, 2024, pp. 329–345.
- [71] A. Hu, L. Russell, H. Yeo, Z. Murez, G. Fedoseev, A. Kendall, J. Shotton, and G. Corrado, “Gaia-1: A generative world model for autonomous driving,” *arXiv preprint arXiv:2309.17080*, 2023.
- [72] X. Wang, Z. Zhu, G. Huang, X. Chen, J. Zhu, and J. Lu, “Drivedreamer: Towards real-world-drive world models for autonomous driving,” in *European Conference on Computer Vision*. Springer, 2024, pp. 55–72.
- [73] J. Yang, S. Gao, Y. Qiu, L. Chen, T. Li, B. Dai, K. Chitta, P. Wu, J. Zeng, P. Luo *et al.*, “Generalized predictive model for autonomous driving,” in *Proceedings of the IEEE/CVF Conference on Computer Vision and Pattern Recognition*, 2024, pp. 14 662–14 672.
- [74] E. Ma, L. Zhou, T. Tang, Z. Zhang, D. Han, J. Jiang, K. Zhan, P. Jia, X. Lang, H. Sun *et al.*, “Unleashing generalization of end-to-end autonomous driving with controllable long video generation,” *arXiv preprint arXiv:2406.01349*, 2024.
- [75] S. Gao, J. Yang, L. Chen, K. Chitta, Y. Qiu, A. Geiger, J. Zhang, and H. Li, “Vista: A generalizable driving world model with high fidelity and versatile controllability,” *arXiv preprint arXiv:2405.17398*, 2024.
- [76] G. Zhao, X. Wang, Z. Zhu, X. Chen, G. Huang, X. Bao, and X. Wang, “Drivedreamer-2: Llm-enhanced world models for diverse driving video generation,” *arXiv preprint arXiv:2403.06845*, 2024.
- [77] Y. Zhang, S. Gong, K. Xiong, X. Ye, X. Tan, F. Wang, J. Huang, H. Wu, and H. Wang, “Bevworld: A multimodal world model for autonomous driving via unified bev latent space,” *arXiv preprint arXiv:2407.05679*, 2024.
- [78] J. Tu, W. Ji, H. Zhao, C. Zhang, R. Zimmermann, and H. Qian, “Driveditfit: Fine-tuning diffusion transformers for autonomous driving,” *arXiv preprint arXiv:2407.15661*, 2024.
- [79] Z. Wu, J. Ni, X. Wang, Y. Guo, R. Chen, L. Lu, J. Dai, and Y. Xiong, “Holodrive: Holistic 2d-3d multi-modal street scene generation for autonomous driving,” *arXiv preprint arXiv:2412.01407*, 2024.
- [80] Y. Chen, Y. Wang, and Z. Zhang, “Drivinggpt: Unifying driving world modeling and planning with multi-modal autoregressive transformers,” *arXiv preprint arXiv:2412.18607*, 2024.
- [81] X. Yang, L. Wen, Y. Ma, J. Mei, X. Li, T. Wei, W. Lei, D. Fu, P. Cai, M. Dou *et al.*, “Drivearena: A closed-loop generative simulation platform for autonomous driving,” *arXiv preprint arXiv:2408.00415*, 2024.
- [82] J. Yang, B. Ivanovic, O. Litany, X. Weng, S. W. Kim, B. Li, T. Che, D. Xu, S. Fidler, M. Pavone *et al.*, “Emernerf: Emergent spatial-temporal scene decomposition via self-supervision,” *arXiv preprint arXiv:2311.02077*, 2023.
- [83] A. Geiger, P. Lenz, and R. Urtasun, “Are we ready for autonomous driving? the kitti vision benchmark suite,” in *Conference on Computer Vision and Pattern Recognition (CVPR)*, 2012.
- [84] J. Behley, M. Garbade, A. Milioto, J. Quenzel, S. Behnke, C. Stachniss, and J. Gall, “SemanticKITTI: A Dataset for Semantic Scene Understanding of LiDAR Sequences,” in *Proc. of the IEEE/CVF International Conf. on Computer Vision (ICCV)*, 2019.
- [85] Y. Cabon, N. Murray, and M. Humenberger, “Virtual kitti 2,” 2020.
- [86] Y. Liao, J. Xie, and A. Geiger, “KITTI-360: A novel dataset and benchmarks for urban scene understanding in 2d and 3d,” *Pattern Analysis and Machine Intelligence (PAMI)*, 2022.
- [87] Y. Cabon, N. Murray, and M. Humenberger, “Virtual kitti 2,” *arXiv preprint arXiv:2001.10773*, 2020.
- [88] H. Turki, J. Y. Zhang, F. Ferroni, and D. Ramanan, “Suds: Scalable urban dynamic scenes,” in *Proceedings of the IEEE/CVF Conference on Computer Vision and Pattern Recognition*, 2023, pp. 12 375–12 385.
- [89] J. Lin, Z. Li, X. Tang, J. Liu, S. Liu, J. Liu, Y. Lu, X. Wu, S. Xu, Y. Yan *et al.*, “Vastgaussian: Vast 3d gaussians for large scene reconstruction,” in *Proceedings of the IEEE/CVF Conference on Computer Vision and Pattern Recognition*, 2024, pp. 5166–5175.
- [90] J. Guo, N. Deng, X. Li, Y. Bai, B. Shi, C. Wang, C. Ding, D. Wang, and Y. Li, “Streetsurf: Extending multi-view implicit surface reconstruction to street views,” *arXiv preprint arXiv:2306.04988*, 2023.
- [91] A. Kirillov, E. Mintun, N. Ravi, H. Mao, C. Rolland, L. Gustafson, T. Xiao, S. Whitehead, A. C. Berg, W.-Y. Lo *et al.*, “Segment anything,” in *Proceedings of the IEEE/CVF international conference on computer vision*, 2023, pp. 4015–4026.
- [92] J. Kulhanek, S. Peng, Z. Kukelova, M. Pollefeys, and T. Sattler, “Wildgaussians: 3d gaussian splatting in the wild,” *arXiv preprint arXiv:2407.08447*, 2024.
- [93] L. Chai, R. Tucker, Z. Li, P. Isola, and N. Snavely, “Persistent nature: A generative model of unbounded 3d worlds,” in *Proceedings of the IEEE/CVF conference on computer vision and pattern recognition*, 2023, pp. 20 863–20 874.
- [94] Z. Chen, G. Wang, and Z. Liu, “Scenedreamer: Unbounded 3d scene generation from 2d image collections,” *IEEE transactions on pattern analysis and machine intelligence*, vol. 45, no. 12, pp. 15 562–15 576, 2023.
- [95] C. H. Lin, H.-Y. Lee, W. Menapace, M. Chai, A. Siarohin, M.-H. Yang, and S. Tulyakov, “Infinicity: Infinite-scale city synthesis,” in *Proceedings of the IEEE/CVF international conference on computer vision*, 2023, pp. 22 808–22 818.
- [96] H. Xie, Z. Chen, F. Hong, and Z. Liu, “Citydreamer: Compositional generative model of unbounded 3d cities,” in *Proceedings of the IEEE/CVF conference on computer vision and pattern recognition*, 2024, pp. 9666–9675.
- [97] —, “Gaussiancity: Generative gaussian splatting for unbounded 3d city generation,” *arXiv preprint arXiv:2406.06526*, 2024.
- [98] J. Ost, F. Mannan, N. Thurey, J. Knodt, and F. Heide, “Neural scene graphs for dynamic scenes,” in *Proceedings of the IEEE/CVF Conference on Computer Vision and Pattern Recognition*, 2021, pp. 2856–2865.
- [99] K. Wu, K. Zhang, Z. Zhang, M. Tie, S. Yuan, J. Zhao, Z. Gan, and W. Ding, “Hgs-mapping: Online dense mapping using hybrid gaussian representation in urban scenes,” *IEEE Robotics and Automation Letters*, 2024.
- [100] G. Song, C. Cheng, and H. Wang, “Gvkf: Gaussian voxel kernel functions for highly efficient surface reconstruction in open scenes,” *Advances in Neural Information Processing Systems*, vol. 37, pp. 104 792–104 815, 2024.
- [101] G. Zhao, C. Ni, X. Wang, Z. Zhu, X. Zhang, Y. Wang, G. Huang, X. Chen, B. Wang, Y. Zhang *et al.*, “Drivedreamer4d: World models are effective data machines for 4d driving scene representation,” *arXiv preprint arXiv:2410.13571*, 2024.
- [102] R. Martin-Brualla, N. Radwan, M. S. Sajjadi, J. T. Barron, A. Dosovitskiy, and D. Duckworth, “Nerf in the wild: Neural radiance fields for unconstrained photo collections,” in *Proceedings of the IEEE/CVF conference on computer vision and pattern recognition*, 2021, pp. 7210–7219.
- [103] M. Tancik, V. Casser, X. Yan, S. Pradhan, B. Mildenhall, P. P. Srinivasan, J. T. Barron, and H. Kretschmar, “Block-nerf: Scalable large scene neural view synthesis,” in *Proceedings of the IEEE/CVF conference on computer vision and pattern recognition*, 2022, pp. 8248–8258.
- [104] Y. Chen, C. Gu, J. Jiang, X. Zhu, and L. Zhang, “Periodic vibration gaussian: Dynamic urban scene reconstruction and real-time rendering,” *arXiv preprint arXiv:2311.18561*, 2023.
- [105] H. Li, J. Li, D. Zhang, C. Wu, J. Shi, C. Zhao, H. Feng, E. Ding, J. Wang, and J. Han, “Vdg: vision-only dynamic gaussian for driving simulation,” *arXiv preprint arXiv:2406.18198*, 2024.
- [106] Z. Yu, H. Wang, J. Yang, H. Wang, Z. Xie, Y. Cai, J. Cao, Z. Ji, and M. Sun, “Sgd: Street view synthesis with gaussian splatting and diffusion prior,” *arXiv preprint arXiv:2403.20079*, 2024.
- [107] C. Peng, C. Zhang, Y. Wang, C. Xu, Y. Xie, W. Zheng, K. Keutzer, M. Tomizuka, and W. Zhan, “Desire-gs: 4d street gaussians for static-dynamic decomposition and surface reconstruction for urban driving scenes,” *arXiv preprint arXiv:2411.11921*, 2024.
- [108] G. Hess, C. Lindström, M. Fatemi, C. Petersson, and L. Svensson, “Splatad: Real-time lidar and camera rendering with 3d gaussian splatting for autonomous driving,” *arXiv preprint arXiv:2411.16816*, 2024.
- [109] F. Lu, Y. Xu, G. Chen, H. Li, K.-Y. Lin, and C. Jiang, “Urban radiance field representation with deformable neural mesh primitives,” in *Proceedings of the IEEE/CVF International Conference on Computer Vision*, 2023, pp. 465–476.
- [110] J. Ost, I. Laradji, A. Newell, Y. Bahat, and F. Heide, “Neural point light fields,” in *Proceedings of the IEEE/CVF Conference on Computer Vision and Pattern Recognition*, 2022, pp. 18 419–18 429.
- [111] X. Zhou, Z. Lin, X. Shan, Y. Wang, D. Sun, and M.-H. Yang, “Drivinggaussian: Composite gaussian splatting for surrounding dynamic autonomous driving scenes,” in *Proceedings of the IEEE/CVF conference on computer vision and pattern recognition*, 2024, pp. 21 634–21 643.
- [112] Y. Chen, J. Zhang, Z. Xie, W. Li, F. Zhang, J. Lu, and L. Zhang, “S-nerf++: Autonomous driving simulation via neural reconstruction

- and generation,” *IEEE Transactions on Pattern Analysis and Machine Intelligence*, 2025.
- [113] H. Zhou, J. Shao, L. Xu, D. Bai, W. Qiu, B. Liu, Y. Wang, A. Geiger, and Y. Liao, “Hugs: Holistic urban 3d scene understanding via gaussian splatting,” in *Proceedings of the IEEE/CVF Conference on Computer Vision and Pattern Recognition*, 2024, pp. 21 336–21 345.
- [114] Q. Tian, X. Tan, Y. Xie, and L. Ma, “Drivingforward: Feed-forward 3d gaussian splatting for driving scene reconstruction from flexible surround-view input,” *arXiv preprint arXiv:2409.12753*, 2024.
- [115] Z. Chen, J. Yang, J. Huang, R. de Lutio, J. M. Esturo, B. Ivanovic, O. Litany, S. Gojcic, S. Fidler, M. Pavone *et al.*, “Omnire: Omni urban scene reconstruction,” *arXiv preprint arXiv:2408.16760*, 2024.
- [116] D. Wei, Z. Li, and P. Liu, “Omni-scene: Omni-gaussian representation for ego-centric sparse-view scene reconstruction,” *arXiv preprint arXiv:2412.06273*, 2024.
- [117] X. Wei, Q. Wu, Z. Zhao, Z. Wu, N. Huang, M. Lu, N. Ma, and S. Zhang, “Emd: Explicit motion modeling for high-quality street gaussian splatting,” *arXiv preprint arXiv:2411.15582*, 2024.
- [118] J. Mao, B. Li, B. Ivanovic, Y. Chen, Y. Wang, Y. You, C. Xiao, D. Xu, M. Pavone, and Y. Wang, “Dreamdrive: Generative 4d scene modeling from street view images,” *arXiv preprint arXiv:2501.00601*, 2024.
- [119] L. Yang, B. Kang, Z. Huang, Z. Zhao, X. Xu, J. Feng, and H. Zhao, “Depth anything v2,” *ArXiv*, vol. abs/2406.09414, 2024.
- [120] M. Oquab, T. Darcet, T. Moutakanni, H. Vo, M. Szafraniec, V. Khali-dov, P. Fernandez, D. Haziza, F. Massa, A. El-Nouby, M. Assran, N. Ballas, W. Galuba, R. Howes, P.-Y. Huang, S.-W. Li, I. Misra, M. Rabbat, V. Sharma, G. Synnaeve, H. Xu, H. Jegou, J. Mairal, P. Labatut, A. Joulin, and P. Bojanowski, “Dinov2: Learning robust visual features without supervision,” 2024.
- [121] B. Cheng, A. Choudhuri, I. Misra, A. Kirillov, R. Girdhar, and A. G. Schwing, “Mask2former for video instance segmentation,” *ArXiv*, vol. abs/2112.10764, 2021.
- [122] S. P. Boyd, N. Parikh, E. Chu, B. Peleato, and J. Eckstein, “Distributed optimization and statistical learning via the alternating direction method of multipliers,” *Found. Trends Mach. Learn.*, vol. 3, pp. 1–122, 2011.
- [123] R. Rombach, A. Blattmann, D. Lorenz, P. Esser, and B. Ommer, “High-resolution image synthesis with latent diffusion models,” in *Proceedings of the IEEE/CVF conference on computer vision and pattern recognition*, 2022, pp. 10 684–10 695.
- [124] N. Ruiz, Y. Li, V. Jampani, Y. Pritch, M. Rubinstein, and K. Aberman, “Dreambooth: Fine tuning text-to-image diffusion models for subject-driven generation,” *2023 IEEE/CVF Conference on Computer Vision and Pattern Recognition (CVPR)*, pp. 22 500–22 510, 2022.
- [125] E. J. Hu, Y. Shen, P. Wallis, Z. Allen-Zhu, Y. Li, S. Wang, L. Wang, W. Chen *et al.*, “Lora: Low-rank adaptation of large language models,” *ICLR*, vol. 1, no. 2, p. 3, 2022.
- [126] Y. Li, Z. Yin, Y. Zheng, H. Lu, T. Kamiya, Y. Nakatoh, and S. Serikawa, “Pose estimation of point sets using residual mlp in intelligent transportation infrastructure,” *IEEE Transactions on Intelligent Transportation Systems*, vol. 24, no. 11, pp. 13 359–13 369, 2023.
- [127] T. Yuan, Y. Mao, J. Yang, Y. Liu, Y. Wang, and H. Zhao, “Presight: Enhancing autonomous vehicle perception with city-scale nerf priors,” in *European Conference on Computer Vision*. Springer, 2024, pp. 323–339.
- [128] H. Yang, S. Zhang, D. Huang, X. Wu, H. Zhu, T. He, S. Tang, H. Zhao, Q. Qiu, B. Lin *et al.*, “Unipad: A universal pre-training paradigm for autonomous driving,” in *Proceedings of the IEEE/CVF Conference on Computer Vision and Pattern Recognition*, 2024, pp. 15 238–15 250.
- [129] W. Zheng, J. Wu, Y. Zheng, S. Zuo, Z. Xie, L. Yang, Y. Pan, Z. Hao, P. Jia, X. Lang *et al.*, “Gaussianad: Gaussian-centric end-to-end autonomous driving,” *arXiv preprint arXiv:2412.10371*, 2024.
- [130] H. Gao, S. Chen, B. Jiang, B. Liao, Y. Shi, X. Guo, Y. Pu, H. Yin, X. Li, X. Zhang *et al.*, “Rad: Training an end-to-end driving policy via large-scale 3dgs-based reinforcement learning,” *arXiv preprint arXiv:2502.13144*, 2025.
- [131] R. Wang, Y. Cao, K. Han, and K.-Y. K. Wong, “A survey on 3d human avatar modeling – from reconstruction to generation,” *arXiv preprint arXiv:2406.04253*, 2024.
- [132] Y. Yang, H. Zhang, A. B. Fernández, S. Alemany, S. Chen, and G. Zhang, “Digitalization of 3-d human bodies: A survey,” *IEEE Transactions on Consumer Electronics*, vol. 70, no. 1, pp. 3152–3166, 2024.
- [133] H. A. Correia and J. H. Brito, “3d reconstruction of human bodies from single-view and multi-view images: A systematic review,” *Computer Methods and Programs in Biomedicine*, vol. 239, p. 107620, 2023.
- [134] L. Lin, Y. Liu, Y. Hu, X. Yan, K. Xie, and H. Huang, “Capturing, reconstructing, and simulating: the urbanscene3d dataset,” in *European Conference on Computer Vision*. Springer, 2022, pp. 93–109.
- [135] Y. Li, L. Jiang, L. Xu, Y. Xiangli, Z. Wang, D. Lin, and B. Dai, “Matrixcity: A large-scale city dataset for city-scale neural rendering and beyond,” in *Proceedings of the IEEE/CVF International Conference on Computer Vision*, 2023, pp. 3205–3215.
- [136] M. Liu, E. Yurtsever, J. Fossaert, X. Zhou, W. Zimmer, Y. Cui, B. L. Zagar, and A. C. Knoll, “A survey on autonomous driving datasets: Statistics, annotation quality, and a future outlook,” *IEEE Transactions on Intelligent Vehicles*, 2024.
- [137] T. Liu, H. Zhao, Y. Yu, G. Zhou, and M. Liu, “Car-studio: learning car radiance fields from single-view and unlimited in-the-wild images,” *IEEE Robotics and Automation Letters*, vol. 9, no. 3, 2024.
- [138] D. Park, R. Ambrus, V. Guizilini, J. Li, and A. Gaidon, “Is pseudo-lidar needed for monocular 3d object detection?” in *Proceedings of the IEEE/CVF International Conference on Computer Vision*, 2021, pp. 3142–3152.
- [139] D. Crandall, A. Owens, N. Snavely, and D. Huttenlocher, “Discrete-continuous optimization for large-scale structure from motion,” in *CVPR 2011*. IEEE, 2011, pp. 3001–3008.
- [140] F. Yu, H. Chen, X. Wang, W. Xian, Y. Chen, F. Liu, V. Madhavan, and T. Darrell, “Bdd100k: A diverse driving dataset for heterogeneous multitask learning,” in *Proceedings of the IEEE/CVF conference on computer vision and pattern recognition*, 2020, pp. 2636–2645.
- [141] H. Caesar, V. Bankiti, A. H. Lang, S. Vora, V. E. Liong, Q. Xu, A. Krishnan, Y. Pan, G. Baldan, and O. Beijbom, “nuscenes: A multimodal dataset for autonomous driving,” *arXiv preprint arXiv:1903.11027*, 2019.
- [142] P. Sun, H. Kretschmar, X. Dotiwalla, A. Chouard, V. Patnaik, P. Tsui, J. Guo, Y. Zhou, Y. Chai, B. Caine *et al.*, “Scalability in perception for autonomous driving: Waymo open dataset,” in *Proceedings of the IEEE/CVF conference on computer vision and pattern recognition*, 2020, pp. 2446–2454.
- [143] M. Cordts, M. Omran, S. Ramos, T. Rehfeld, M. Enzweiler, R. Benenson, U. Franke, S. Roth, and B. Schiele, “The cityscapes dataset for semantic urban scene understanding,” in *Proc. of the IEEE Conference on Computer Vision and Pattern Recognition (CVPR)*, 2016.
- [144] B. Xiong, N. Zheng, J. Liu, and Z. Li, “Gauu-scene v2: Assessing the reliability of image-based metrics with expansive lidar image dataset using 3dgs and nerf,” *arXiv preprint arXiv:2404.04880*, 2024.
- [145] P. Xiao, Z. Shao, S. Hao, Z. Zhang, X. Chai, J. Jiao, Z. Li, J. Wu, K. Xiong, K. Jiang *et al.*, “Pandaset: Advanced sensor suite dataset for autonomous driving,” in *2021 IEEE international intelligent transportation systems conference (ITSC)*. IEEE, 2021, pp. 3095–3101.
- [146] M. Alibeigi, W. Ljungbergh, A. Tonderski, G. Hess, A. Lilja, C. Lindström, D. Motorniuk, J. Fu, J. Widahl, and C. Petersson, “Zenseact open dataset: A large-scale and diverse multimodal dataset for autonomous driving,” in *Proceedings of the IEEE/CVF International Conference on Computer Vision*, 2023, pp. 20 178–20 188.
- [147] E. Son, J. Choi, J. Song, Y. Jin, and S. J. Lee, “Monocular depth estimation from a fisheye camera based on knowledge distillation,” *Sensors*, vol. 23, no. 24, p. 9866, 2023.
- [148] X. Weng, Y. Man, J. Park, Y. Yuan, M. O’Toole, and K. M. Kitani, “All-in-one drive: A comprehensive perception dataset with high-density long-range point clouds,” 2021.
- [149] A. Ligocki, A. Jelinek, and L. Zalud, “Brno urban dataset-the new data for self-driving agents and mapping tasks,” in *2020 IEEE International Conference on Robotics and Automation (ICRA)*. IEEE, 2020, pp. 3284–3290.
- [150] M.-F. Chang, J. Lambert, P. Sangkloy, J. Singh, S. Bak, A. Hartnett, D. Wang, P. Carr, S. Lucey, D. Ramanan *et al.*, “Argoverse: 3d tracking and forecasting with rich maps,” in *Proceedings of the IEEE/CVF conference on computer vision and pattern recognition*, 2019, pp. 8748–8757.
- [151] B. Wilson, W. Qi, T. Agarwal, J. Lambert, J. Singh, S. Khandelwal, B. Pan, R. Kumar, A. Hartnett, J. K. Pontes *et al.*, “Argoverse 2: Next generation datasets for self-driving perception and forecasting,” *arXiv preprint arXiv:2301.00493*, 2023.
- [152] P. Bojanowski, A. Joulin, D. Lopez-Paz, and A. Szlam, “Optimizing the latent space of generative networks,” *arXiv preprint arXiv:1707.05776*, 2017.
- [153] R. Zhang, P. Isola, A. A. Efros, E. Shechtman, and O. Wang, “The unreasonable effectiveness of deep features as a perceptual metric,” *2018 IEEE/CVF Conference on Computer Vision and Pattern Recognition*, pp. 586–595, 2018.
- [154] S. T. Barratt and R. Sharma, “A note on the inception score,” *ArXiv*, vol. abs/1801.01973, 2018.

- [155] M. Heusel, H. Ramsauer, T. Unterthiner, B. Nessler, and S. Hochreiter, “Gans trained by a two time-scale update rule converge to a local nash equilibrium,” in *Neural Information Processing Systems*, 2017.
- [156] S. N. I. Rosli and M. I. E. Zulkifly, “Neutrosophic bicubic bezier surface approximation model for uncertainty data,” *MATEMATIKA*, vol. 39, no. 3, p. 281–291, Dec. 2023.
- [157] A. Arnal and J. Monterde, “Bézier-smart surfaces of arbitrary degree,” *Journal of Computational and Applied Mathematics*, vol. 457, p. 116253, 2025.
- [158] Y.-X. Hao and W.-Q. Fei, “Construction of bézier surfaces with minimal quadratic energy for given diagonal curves,” *Journal of Computational and Applied Mathematics*, vol. 446, p. 115854, 2024.
- [159] X. Zou, S. B. Lo, R. Sevilla, O. Hassan, and K. Morgan, “The generation of 3d surface meshes for nurbs-enhanced fem,” *Computer-Aided Design*, vol. 168, p. 103653, 2024.
- [160] N. Grillanda, A. Chiozzi, G. Milani, and A. Tralli, “Nurbs solid modeling for the three-dimensional limit analysis of curved rigid block structures,” *Computer Methods in Applied Mechanics and Engineering*, vol. 399, p. 115304, 2022.
- [161] M. Yu, T. Lu, L. Xu, L. Jiang, Y. Xiangli, and B. Dai, “Gsd: 3dgs meets sdf for improved neural rendering and reconstruction,” *Advances in Neural Information Processing Systems*, vol. 37, pp. 129 507–129 530, 2024.
- [162] X. Lyu, Y.-T. Sun, Y.-H. Huang, X. Wu, Z. Yang, Y. Chen, J. Pang, and X. Qi, “3dgsr: Implicit surface reconstruction with 3d gaussian splatting,” *ACM Transactions on Graphics (TOG)*, vol. 43, no. 6, pp. 1–12, 2024.
- [163] H. Xiang, X. Li, X. Lai, W. Zhang, Z. Liao, K. Cheng, and X. Liu, “Gaussianroom: Improving 3d gaussian splatting with sdf guidance and monocular cues for indoor scene reconstruction,” *arXiv preprint arXiv:2405.19671*, 2024.
- [164] P. Wang, Y. Liu, Z. Chen, L. Liu, Z. Liu, T. Komura, C. Theobalt, and W. Wang, “F2-nerf: Fast neural radiance field training with free camera trajectories,” in *Proceedings of the IEEE/CVF Conference on Computer Vision and Pattern Recognition*, 2023, pp. 4150–4159.
- [165] A. Knapitsch, J. Park, Q.-Y. Zhou, and V. Koltun, “Tanks and temples: Benchmarking large-scale scene reconstruction,” *ACM Transactions on Graphics (TOG)*, vol. 36, no. 4, pp. 1–13, 2017.
- [166] V. Rudnev, M. Elgharib, W. Smith, L. Liu, V. Golyanik, and C. Theobalt, “Nerf for outdoor scene relighting,” in *European Conference on Computer Vision*. Springer, 2022, pp. 615–631.
- [167] N. Snavely, S. M. Seitz, and R. Szeliski, “Photo tourism: exploring photo collections in 3d,” *ACM siggraph 2006 papers*, pp. 835–846, 2006.
- [168] P. Liu, Y. Zhang, H. Wang, M. K. Yip, E. S. Liu, and X. Jin, “Real-time collision detection between general sdfs,” *Computer Aided Geometric Design*, 2024.
- [169] M. Macklin, K. Erleben, M. Müller, N. Chentanez, S. Jeschke, and Z. Corse, “Local optimization for robust signed distance field collision,” *Proc. ACM Comput. Graph. Interact. Tech.*, 2020.
- [170] X. Zhu, Y. Xin, S. Li, H. Liu, C. Xia, and B. Liang, “Efficient collision detection framework for enhancing collision-free robot motion,” *arXiv preprint arXiv:2409.14955*, 2024.
- [171] X. Zheng, Y. Liu, P. Wang, and X. Tong, “Sdf-stylegan: implicit sdf-based stylegan for 3d shape generation,” in *Computer Graphics Forum*, vol. 41, no. 5. Wiley Online Library, 2022, pp. 52–63.
- [172] M. Li, Y. Duan, J. Zhou, and J. Lu, “Diffusion-sdf: Text-to-shape via voxelized diffusion,” in *Proceedings of the IEEE/CVF conference on computer vision and pattern recognition*, 2023, pp. 12 642–12 651.